# OPTIMIZATION OF THE ROUTINE GROWTH OF $UO_2$-W EUTECTICS

A THESIS

Presented to

The Faculty of the Division of Graduate Studies and Research

by

Raymond William Barkalow

In Partial Fulfillment

of the Requirements for the Degree

Master of Science in Ceramic Engineering

Georgia Institute of Technology

February 1977

# OPTIMIZATION OF THE ROUTINE GROWTH OF $UO_2$-W EUTECTICS

Approved:

Alan T. Chapman, Chairman

Joseph K. Cochran, Jr.

James F. Benzel

Mar. 8, 1977
Date

# ACKNOWLEDGEMENTS

The author wishes to express his sincere appreciation and gratitude to Dr. A. T. Chapman for his continued support and suggestions while acting as adviser, and to Dr. J. K. Cochran and Dr. J. F. Benzel for their advice while serving on the reading committee.

Special thanks is due to Mr. M. Watson for his assistance, and to Mr. W. Ohlinger and Mr. D. Hill for feedback concerning sample performance.

Compliments are due to my wife, Michele, for providing the support and calming influence necessary during the composition of this thesis.

TABLE OF CONTENTS

TABLE OF CONTENTS (continued)

# LIST OF TABLES

# LIST OF ILLUSTRATIONS

LIST OF ILLUSTRATIONS (continued)

## SUMMARY

Direct rf induction heating and the internal molten zone technique were used to unidirectionally solidify a variety of $UO_2$-W composite growth samples. Structures yielding from 1.4 to 30 million, less than one micrometer diameter, tungsten fibers per square centimeter, in a urania matrix were produced. Parameters affecting composite growth were investigated, and experimental techniques were developed to optimize conditions and alleviate problems encountered.

# CHAPTER I

## INTRODUCTION

Several methods have been used to unidirectionally solidify oxide-metal mixtures to produce composites with an ordered microstructure composed of sub-micron metal rods or platelets in an oxide matrix. To date the largest and most uniform oxide-metal composites reported have been grown using the direct rf coupling floating internal molten zone technique. The main advantage of this technique is that the molten zone is self contained by the unmelted skin which eliminates the containment and contamination problems inherent in other methods. Its major disadvantages include limited sample size, and limited sample materials, because only a few refractory oxides possess sufficient high temperature electrical conductivity to support eddy current heating and high enough melting points to allow radiation cooling of the skin.

Prior to this investigation, ordered oxide-metal structures had been achieved using the direct rf coupling technique in many systems, including the $UO_2$-metal (Ta or W), stabilized $ZrO_2$-W, stabilized $HfO_2$-W systems, and rare-earth oxide-metal systems. Each of these presents inherent materials problems however. It has thus far been impossible, in the hafnia and zirconia systems, to produce crack-free samples even with proper stabilization. In the $UO_2$ systems, oxide stoichiometry is very critical and must be precisely controlled to obtain good growth.

The rare-earth oxides sometimes display post-growth destruction through hydration.

To date, the major application of in-situ oxide-metal composites is as cathodes in field emission studies, where the structural integrity of samples is critical. The $UO_2$-W system was selected for further study because the most uniform and controllable fiber geometries have been produced in this system.

The purpose of this investigation was to identify the parameters and problems associated with $UO_2$-W composite growth and to produce usable fiber geometries on a routine basis.

# CHAPTER II

## SURVEY OF LITERATURE

This chapter is a review of literature related to the unidirectional solidification of $UO_2$-W composites. The basic theory behind induction heating is discussed, along with oxide and oxide-metal systems that were melted using direct induction heating. A summary of the coupled zone theory, and brief comments on $UO_2$ are also given.

### Induction Heating

It is well known that when an electrically conductive material is placed in a time-varying magnetic field, induction heating occurs (1). The most commonly used technique for producing the magnetic field is to pass an alternating electric current through a coil. If the material to be heated is centered in this coil, the magnetic field will induce circulating "eddy" currents (2) within the material, and resistance heating will occur due to $I^2R$ losses, as shown in Figure 1. The magnitude of these induced currents, and hence, the heating effect (3), is determined by the effective magnitude of the induced voltages and the impedance of the material.

The efficiency of power absorption by a solid, cylindrical specimen from an alternating magnetic field is related to A*, which is the ratio of specimen radius and the "skin depth" (1). Since the current distribution in the workpiece decreases exponentially from the surface to the interior as depicted in Figure 2, the skin depth is defined as

(a)

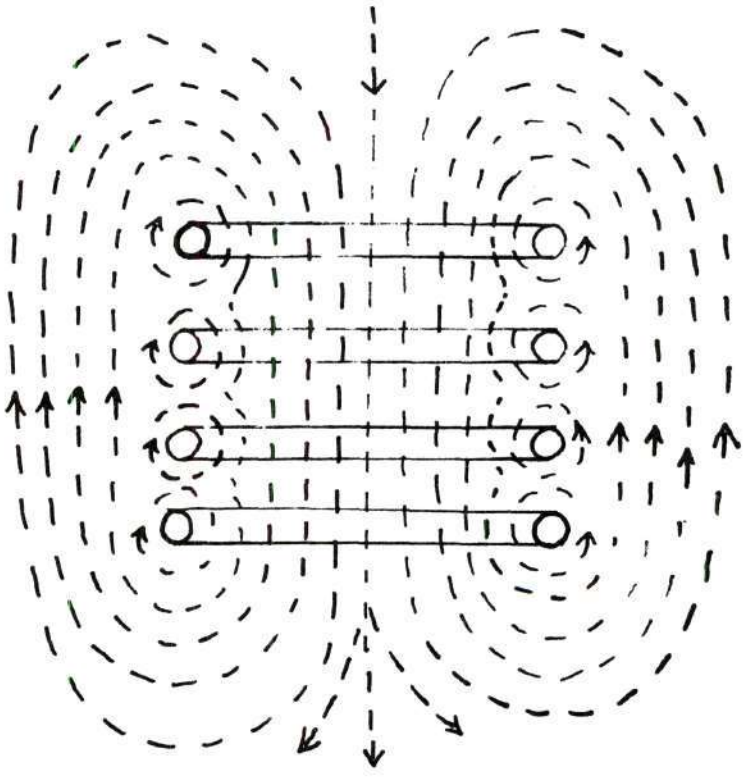

(b)

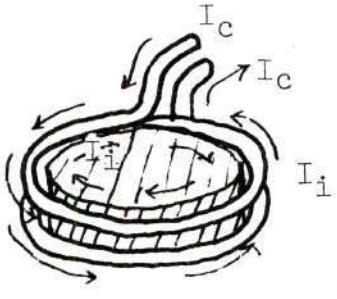


Figure 1 (a). Electromagnetic Field Established Around The Conductor when Alternating Electric Current Flows in a Conductor

(b). The Induced Current is Determined by the Strength of the Alternating Magnetic Field and the Spacing Between the Workpiece and the Coil, where $I_c$ Is Coil Current and $I_i$ Is the Induced Current in Workpiece

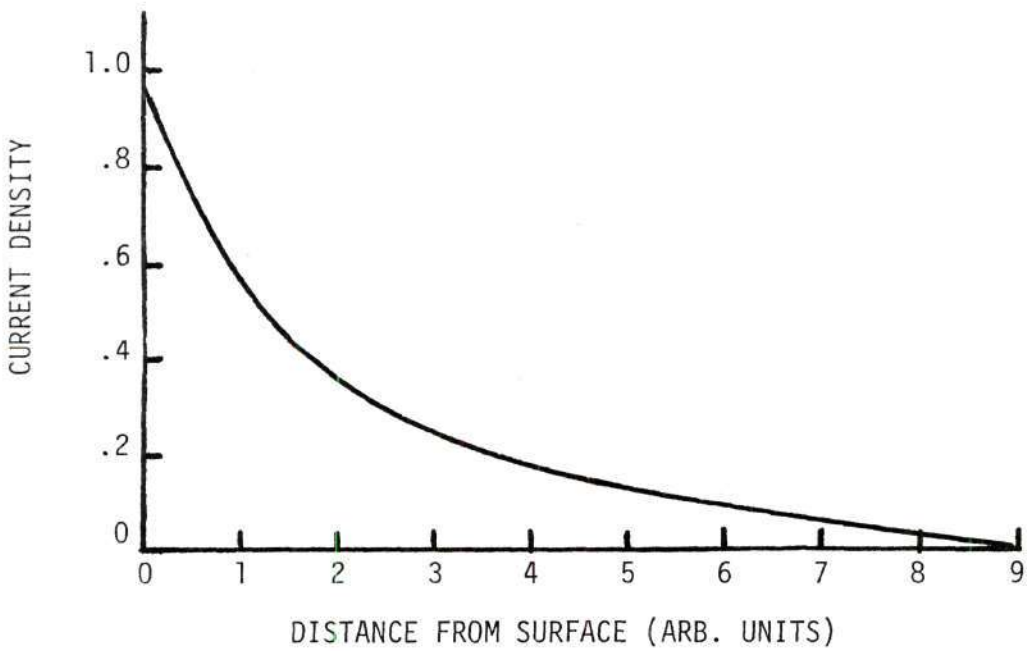


Figure 2. Current Density in a Solid Cylindrical Conductor Centered in an Oscillating Magnetic Field

the depth below which the current density has been reduced to 1/e or approximately 37% of the current density at the surface. Watson (4) states that an equation for the skin depth D has been given as:

$$D = \frac{1}{2\pi}\sqrt{\frac{10^9}{f\sigma}} \qquad \text{(Eq.1)}$$

Where D is in centimeters, f is the frequency in hertz, and $\sigma$ is the electrical conductivity in mho/cm. The power absorption efficiency of the workpiece can be calculated (5) as a function of A*, as shown in Figure 3.

It has been calculated (6) that for a 35 mm diameter $UO_2$ pellet to be heated efficiently at room temperature, the necessary frequency should be approximately $10^{10}$ hertz. Unfortunately, since frequencies above about 30 MHz are difficult to contain due to arcing between turns of the coil and atmospheric gas ionization problems (3,4), it would be impractical, if not impossible, to obtain efficient induction heating. Equation 1 shows that by increasing the electrical conductivity, $\sigma$, of the workpiece, it would be possible to use a lower frequency to attain heating. Gayet (6) calculated that by preheating the $UO_2$ pellet to 1300°C, its conductivity would be increased sufficiently to permit the melting of the oxide using a more practical five MHz frequency.

## Melting of Oxide and Oxide-Metal Systems Utilizing Direct Induction Heating

Molten zones were initiated by Hill (7) in ingots of $CeO_2$, $BaTiO_3$, $Cr_2O_3$, $TiO_2$, and $Ca_{0.1}Zr_{0.9}O_{1.9}$ using frequencies ranging from 6 to 30 MHz. Chapman et al. (8) were able to melt several oxide compounds

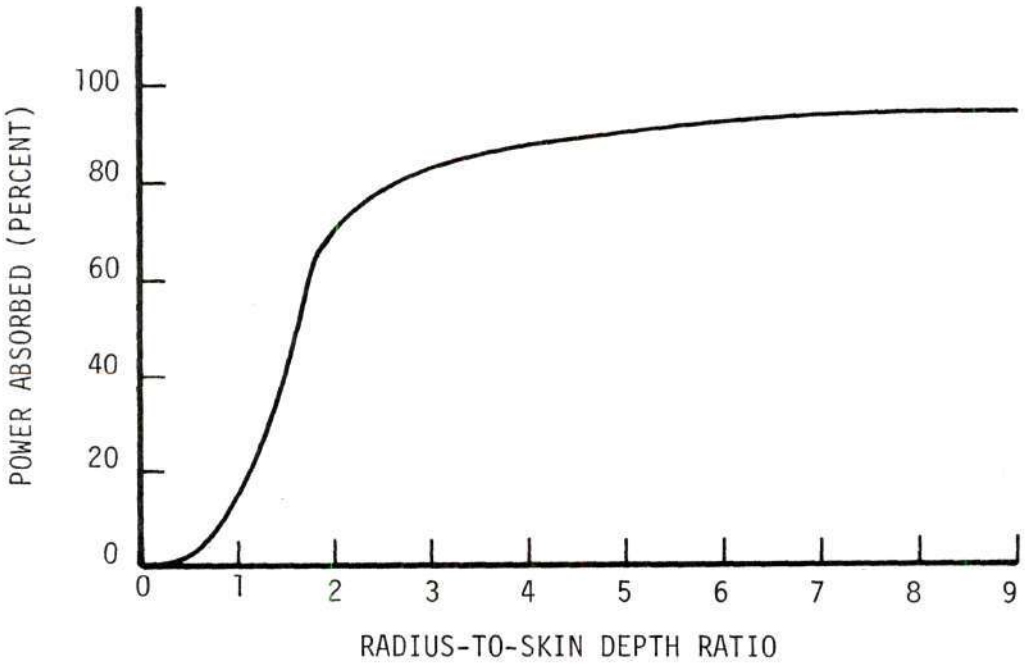


Figure 3. Power Absorbed from an Oscillating Magnetic Field As A Function of A*, the Radius-to-Skin Depth Ratio

including: $NiO:TiO_2$, $TiO_{2-x}$, $Cr_2O_3$ + 40 w/o $ZrO_2$, and ZnO + 20 w/o $Nb_2O_5$.

$UO_2$ single crystals up to 5 cm long and 1 cm diameter were produced by Chapman and Clark (9) by melting a polycrystalline rod and resolidifying it unidirectionally. They utilized a radio frequency generator operating in the range of 3 to 10 MHz. Barkalow (10) found that single crystals of $Y_2O_3$-stabilized $ZrO_2$ could be grown in a similar manner.

The unidirectional solidification of several other oxide-oxide systems have been reported (3,11,12), including: (CaO, MgO, SrO, and BaO)-$UO_2$; CaO-NiO, $Al_2O_3$- NiO; MgO-$AgAl_2O_4$; $Al_2O_3$-$Y_2Al_5O_{12}$; $ZrO_2$-$Y_2O_3$; $ZrO_2$-MgO; $BaTiO_3$-$COFe_2O_4$, $Al_2O_3$-$ZrO_2(Y_2O_3)$; piezomagnetic spinel-piezoelectric perovskite eutectics in the Fe-Co-Ti-Ba-O system; and $BaNb_2O_6$-$SrNb_2O_6$.

During the study made by Chapman et al. (8), a number of oxide-metal systems were induction melted and solidified. These included: $UO_2$-W, $UO_2$-Ta, $HfO_2(Y_2O_3)$-W, $ZrO_2(Y_3O_2)$-W, $Y_2O_3(CeO_2)$-W or Mo, $Gd_2O_3$ $(CeO_2)$-W or Mo, $Nd_2O_3(CeO_2)$-W or Mo, and $La_2O_3(CeO_2)$-W or Mo. Those investigators were able to establish some of the parameters controlling the growth of oxide-metal composites which are listed in Table 1.

Using direct induction heating $UO_2$-Ta composites were grown by Jen (13) at a frequency of about four MHz. Very limited metal fiber growth was observed in $UO_2$-Mo experiments, presumably due to the low solubility of the metal in the melt. No fibers were realized in the $UO_2$-Nb system, which was attributed to the very high vapor pressure of the metal at the melting temperature of $UO_2$. Watson et al. (14)

Table 1. Parameters Influencing Composite Growth in Refractory Oxide-Metal Systems After Chapman et al (8)

1. Oxide-metal ratio
2. Growth rate
3. Metal powder characteristics
4. High-temperature electrical conductivity
5. Rf frequency
6. Mixing of the liquid (sample rotation)
7. Melting (eutectic) temperature
8. Preheat temperature
9. Sample density
10. Sample rf-coil geometry
11. Quantity of liquid and void size
12. Oxygen partial pressure
13. Pre- and post-heater separation
14. Vapor pressure
15. Variable oxide stoichiometry

succeeded in producing an ordered microstructure of W fibers in CaO-stabilized $ZrO_2$ using the internal floating zone technique developed by Chapman (8,9). Large areas of composite growth were not achieved, however, due to the reaction of the CaO and W. Later, Watson (4) successfully grew large areas of $ZrO_2$-W composite by utilizing $Y_2O_3$ as the stabilizing agent.

In a more recent tabulation, Benzel (11) listed several other oxide-metal systems in which ordered eutectic growth was realized: $Cr_2O_3$-(Mo, Re or W), MgO-W; ($Er_2O_3$ or $Ho_2O_3$ )-$CeO_2$-(Mo or W), $CeO_2$-Mo or W; and $Y_2O_3$-(Mo or W), $Ta_2O_5$-Ta, $ZrO_2$-(Zr or W), $HfO_2$-$HfO_2$-Hf, $Al_2O_3(Cr_2O_3)$-W, $Al_2O_3$-$ZrO_2(Y_2O_3)$-W, ($Gd_2O_3$ or $Y_2O_3$)-$CeO_2$-Ta, $Y_2O_3$-$CeO_2$-Y, $Cr_2O_3$-$Al_2O_3$-Cr.

Most recently, Briggs and Hart (15) studied the following systems revealing well-defined eutectics: $CeO_2$-Mo or W, $Sm_2O_3$-W, $Sm_2O_3(CeO_2)$-W, $Y_2O_3$-Ta, and $Y_2O_3(CeO_2)$-Mo.

## Coupled Zone Theory

The theory of coupled zone growth is based on a concept developed by Scheil (16), which was later revised by Tiller (17) and Hogan (18). The concept assumed that the solidification rate of any solid phase is proportional to the degree of supersaturation of the melt with respect to that phase. A degree of supersaturation is necessary for growth to occur and the rate of solidification increases with increasing supersaturation. Supersaturation can be produced by a compositional change or by supercooling.

The coupled zone as defined by Brady (19) and named by Kofler (20)

is a region below the eutectic temperature into which supercooling can lower the temperature of the liquid. In this region there is a compositional range from which eutectic structures can be solidified on either side of the equilibrium eutectic point (Figure 4). Solidification of the melt produces a normal eutectic structure.

Slightly below the eutectic temperature the growth rate of the phases will be equal, and they can grow with a common crystallization front with a "pure" eutectic microstructure. With increasing supercooling the growth rate should increase, but processes occur which produce a difference in the growth rate for both phases.

A binary phase diagram for mutually insoluble metals A and B is represented in Figure 4. The liquidus lines have been extended below the eutectic point. These are saturation curves passing through $C_{ma}$ and $C_{mb}$ representing the compositions and temperatures at which the liquid is just saturated with respect to metals A and B, respectively.

The degree of supersaturation of the melt will increase at different rates for a given melt composition unless the saturation curves are symmetrical. For example, if a melt of composition $C_e$ is supercooled to $T_o$, it will be supersaturated with respect to A in proportion to the distance $C_{ma}$-$C_e$, and with respect to B in proportion to the smaller distance $C_e$-$C_{mb}$.

Hence, the solid phase A should grow much more rapidly than B at $T_o$. The melt composition would have to shift to the intermediate value $C_o$ to produce equal supersaturation and therefore equal growth rates.

Kofler (20) described two possible types of coupled regions as shown in Figures 4 and 5. In Figure 4 the coupled region is almost

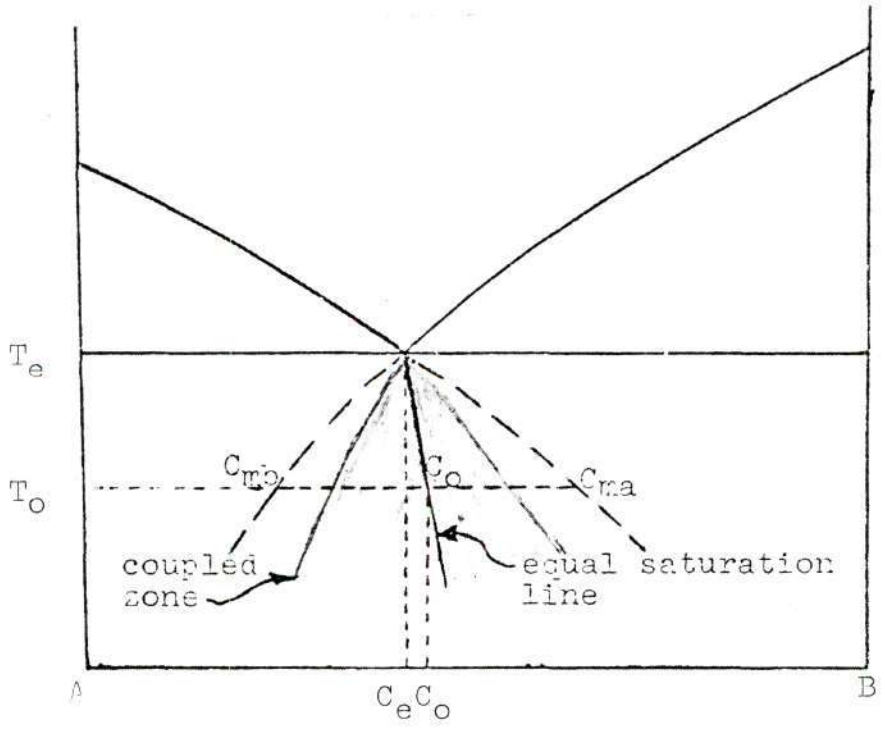


Figure 4. The Coupled Zone and Equal Saturation Line in a System in which the Extended Liquidus Lines are Roughly Symmetrical about the Eutectic Point. The Distance $C_{mb}$-$C_o$ Equals the Distance $C_{ma}$-$C_o$, After Watson(4).

symmetrical so that a normal eutectic structure would be achieved. Alloys either side of $C_e$ would solidify as pure eutectic if enough undercooling were achieved. Figure 5 represents a different situation, which is typical of systems of materials with widely-differing melting temperatures. The coupled zone is skewed toward the higher melting component instead of centered below the eutectic point. The skew is caused by the greater degree of supercooling of the liquid with the higher melting point. Due to the unequal undercooling, even if the saturation of both phases is the same, the solidification rates will be different. The inequality of solidification rates at equal supersaturation produces the displacement of the coupled zone to a region in which the rates are equal. That, in turns, leads to a liquid that is supersaturated in one phase only. Upon cooling the system represented in Figure 5, the B phase would be nucleated and grown dendritically until the liquid composition was depleted in that material. The A phase would then solidify as a "halo" around the B dendrite. The liquid composition would then move back into the coupled zone, providing for the solidification of the pure eutectic. More detailed summaries are given by Watson (4) and Graves (21).

## Urania

At elevated temperatures, uranium dioxide exists as a single-phase material over a broad range of stoichiometry. In the oxygen-deficient region, Latta and Dryxell (22) report a monotectic at an oxygen-to-uranium ratio (O/U) of about 1.46 and a temperature of 2425°C. In the oxygen-rich region, they were confronted by extensive interaction between the $UO_2$ and the tungsten or rhenium sample enclosures. Post-

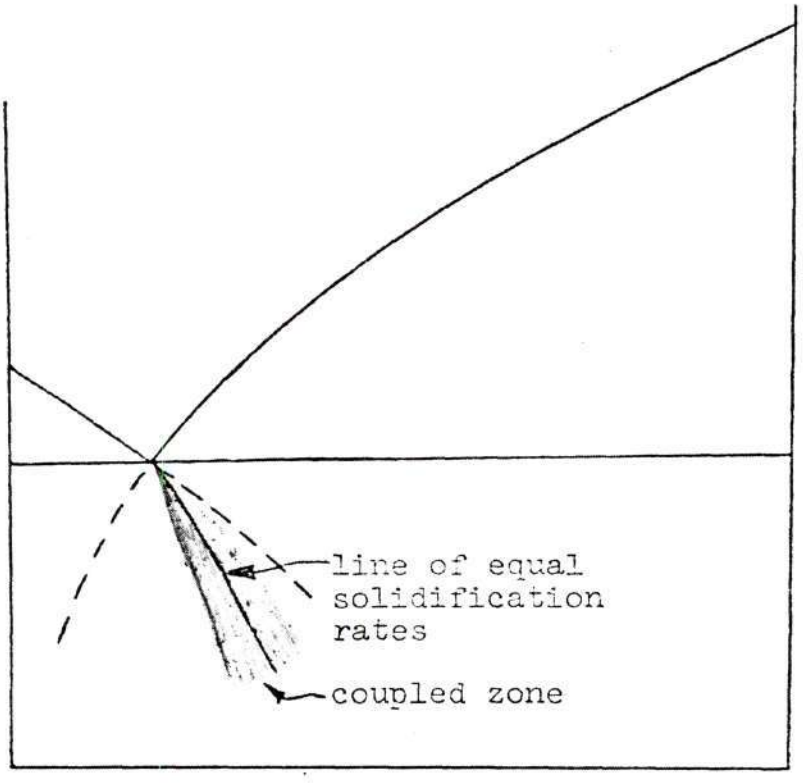


Figure 5. The Skewed Coupled Zone in Systems with A Symmetrical Liquidus Lines, After Watson (4).

test microscopic examination of some of their tungsten-encapsulated samples revealed the presence of a violet or blue phase having a Perovskite structure to which they assigned the formula $U_xWO_3$. During that study, stoichiometric $UO_2$ was found to have a vapor pressure of about ten torr at its congruent melting temperature, 2865°C. Their relationship between the O/U ratio and W solubility in molten urania is presented in Figure 6.

Hagemark and Broli (23) used a thermobalance to determine the non-stoichiometry of $UO_{2\pm x}$ and $U_3O_{8-z}$ as a function of the partial oxygen pressure over a temperature range of 900 to 1500°C. They utilized CO-$CO_2$ and $O_2$-Ar mixtures to obtain the proper atmospheric oxygen potentials. Values for the partial free enthalpy of oxygen, as well as the enthalpy and entropy, were given.

A comparable study was conducted by Javed (24) on hypostoichiometric urania using $H_2$-$H_2O$ gas mixtures to control oxygen partial pressures.

Existing experimental data describing equilibrium phase relations for $UO_{2+x}$ from 1000°C up to and including the molten oxide were recently presented by Chapman (25), who used selected data to construct a partial O/U phase diagram. This work established a relationship between atmospheric oxygen partial pressure and the composition of the oxide, as shown in Figure 7.

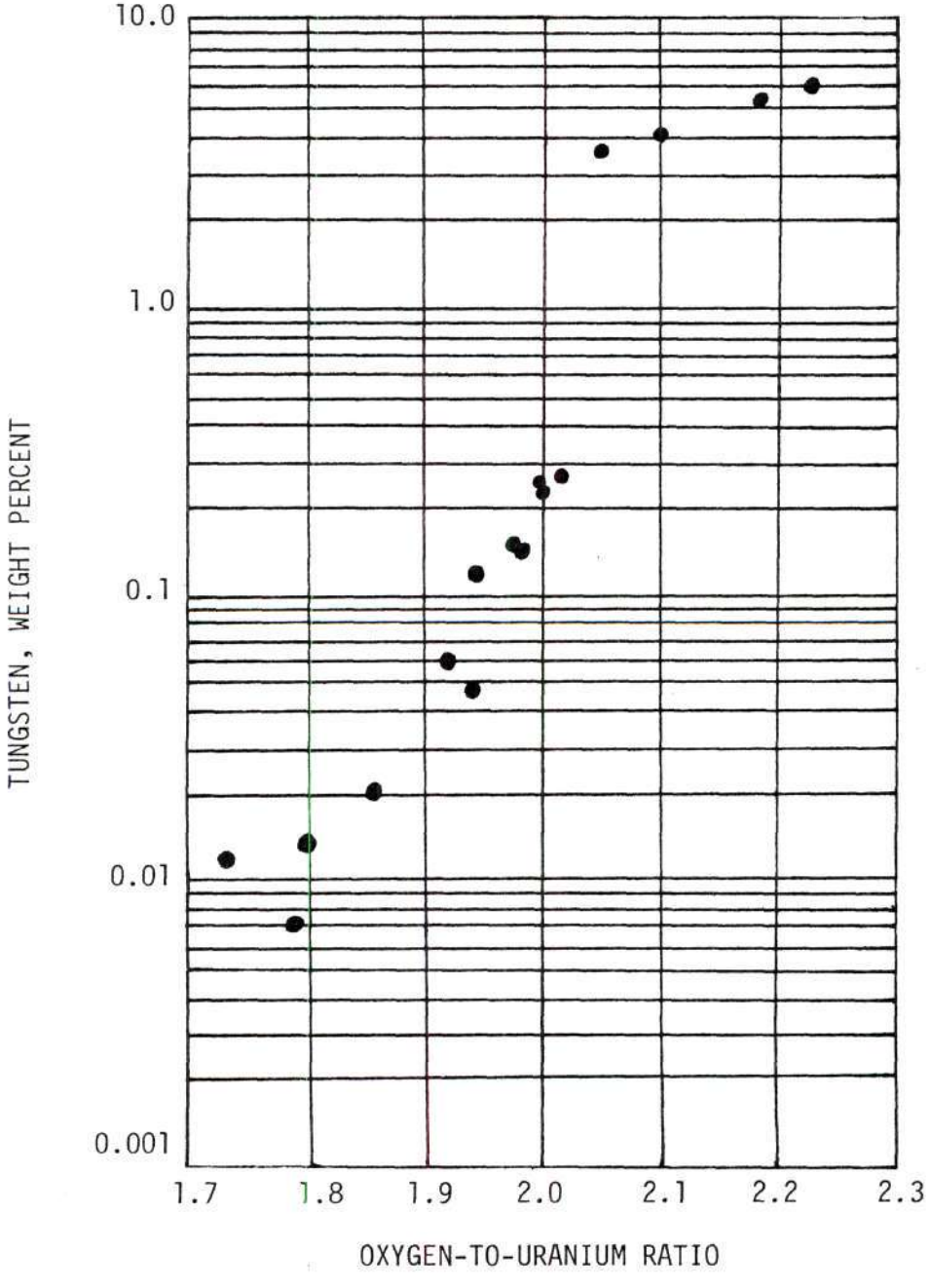


Figure 6. Tungsten Solubility in Molten Urania as a Function of O/U Ratio, After Latta and Fryxell (22)

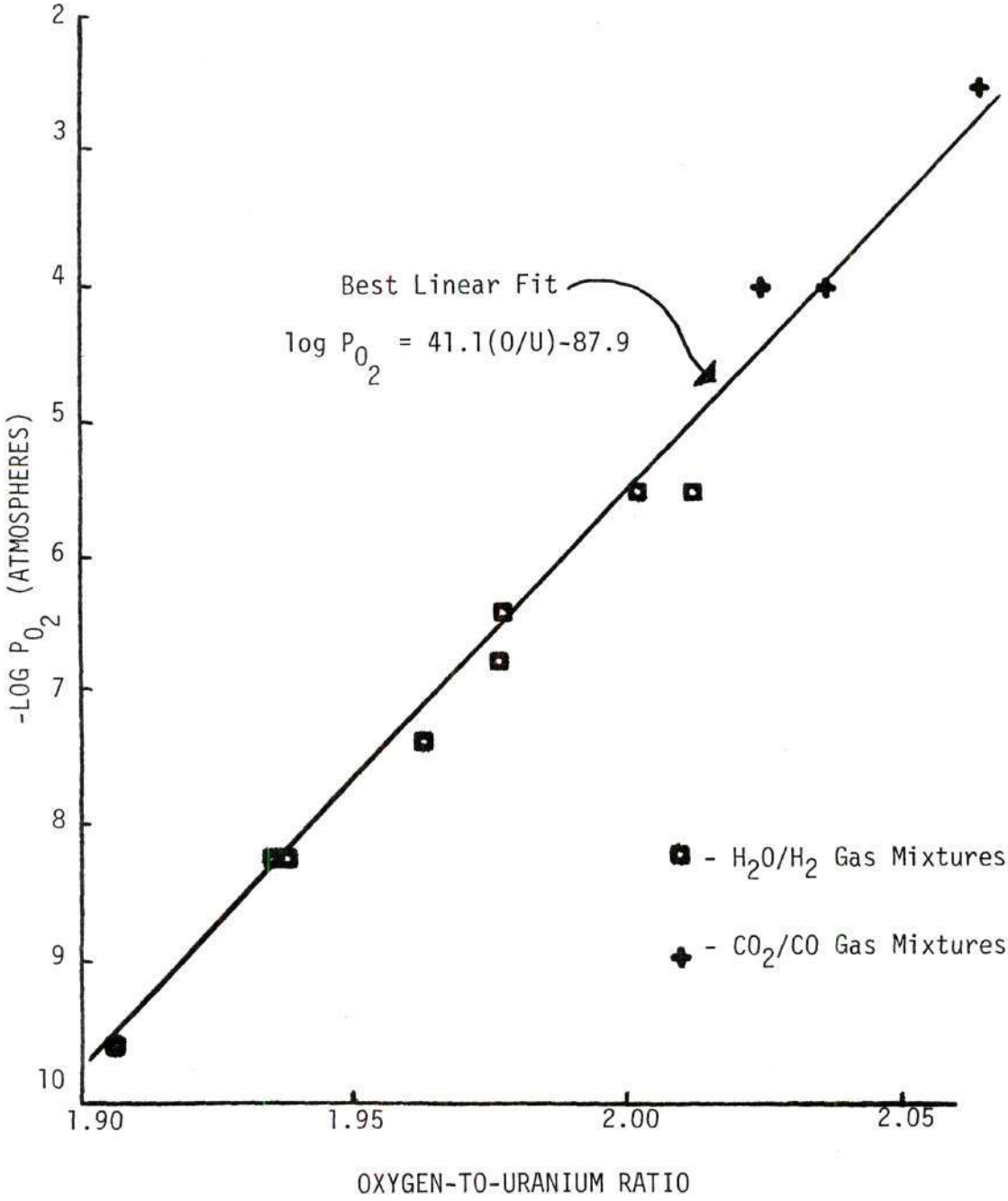


Figure 7. Equilibrium Oxygen Partial Pressure As A Function of the Composition of Molten Urania, After Chapman (25).

# CHAPTER III

# EQUIPMENT

The equipment used for producing $UO_2$-W composites consisted of a Lepel high frequency induction heating unit and the apparatus necessary for control of the unidirectional solidification process. Since this equipment is vital in the production of composites, it will be described in detail. Equipment used for sample preparation and examination will also be discussed.

## Induction Heating Unit

A Lepel high frequency generator, model number T-10-3-DF1-E-HW, type T-1003-58, (Figure 8) was used to supply power for induction heating. The generator is rated at 10 kilowatt output, capable of operating in the frequency ranges of 2.5 to 8 MHz and 15 to 35 MHz. The proper selection of coils and capacitors that can be interchanged within the unit determines the frequency of operation. A variable grid coil capable of adjustment during operation made possible a fine tuning of the unit to match the work load being heated. Meters on the generator's control panel showed the filament voltage, grid current, plate current, plate voltage, and control current. The plate current and voltage were used to record and control the power settings used.

The work load consisted of a load coil and the material to be heated. The load coil was constructed from 9.5 mm diameter copper tubing. The coil was an 9.25 cm tall, 5 and 1/2 turn helix with an in-

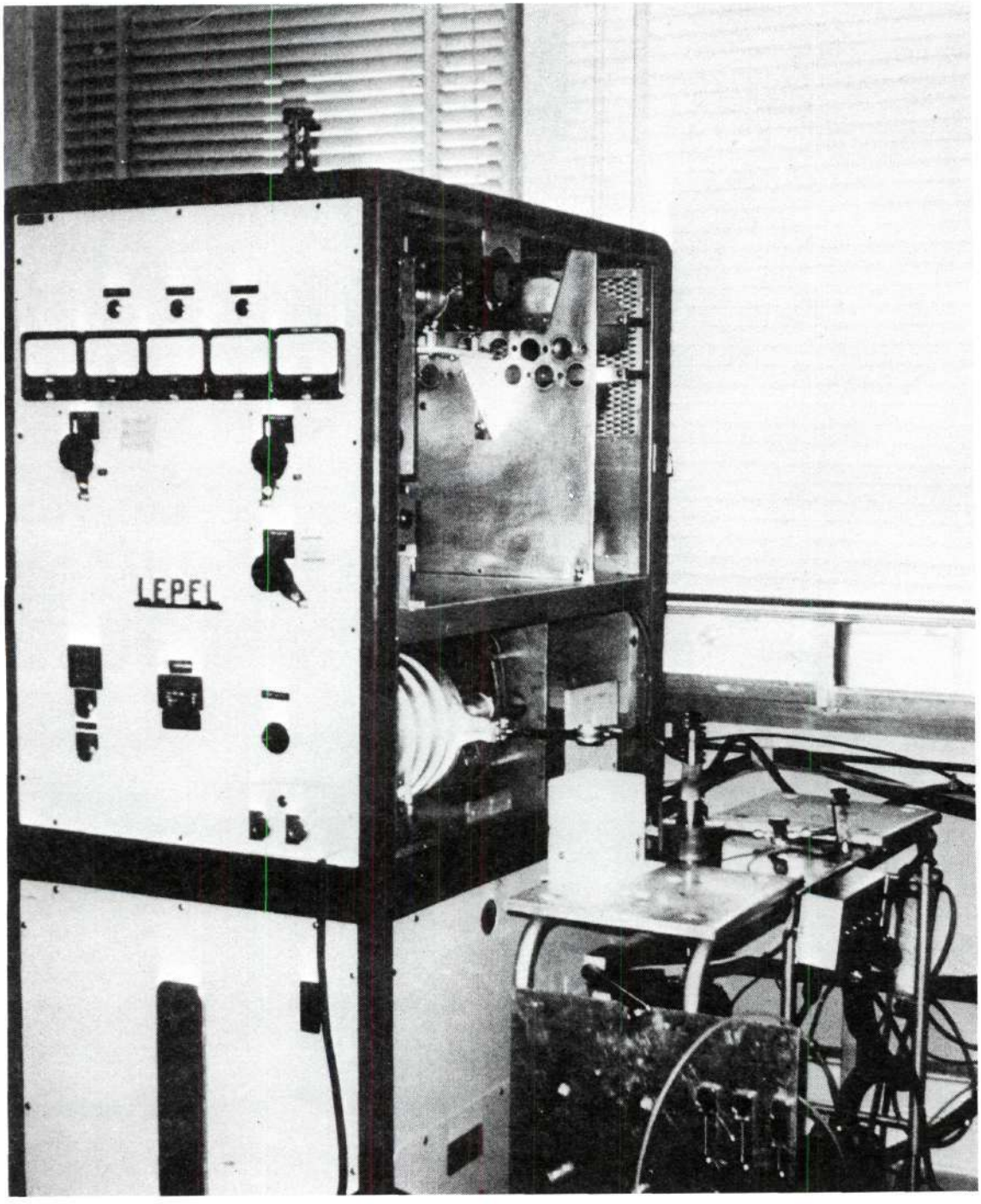


Figure 8. Overall View of the Dual Frequency RF Generator and Composite Growth Equipment

side diameter of 6.67 cm. Connections in the generator supplied cooling water which circulated through the coil.

## Unidirectional Solidification Apparatus

The facilities, in addition to the Lepel generator, for oxide-metal composite growth were developed as part of this investigation and other research being done concerning composite growth. The growth facility was mounted on a table that could be manually raised or lowered by means of a hand crank. Mounted below the table were a hydraulic cylinder for sample movement and a vacuum pump. On the side of the table were the controls, for the hydraulic system, and valves and flow meters used for atmosphere regulation.

Figure 9 shows a schematic diagram of the growth facilities mounted on the table. A brass support held a silica atmosphere containment tube and a ceramic support held the molybdenum preheater tube. A steel rod extended from the hydraulic cylinder up through the table, the brass support, and the preheater tube. On the end of the rod was an alumina tube used to support the sample. Movement of the table raised or lowered the silica tube and preheater tube independent of the steel rod and sample. Movement of the sample was accomplished by the hydraulic cylinder. A system of needle and shut off valves controlled the flow of the hydraulic fluid so that the sample could be either raised or lowered at controlled rates in the range from near zero up to about twenty centimeters per hour.

Control of the atmosphere was accomplished by the use of a vacuum pump, tanks of nitrogen, carbon monoxide, and carbon dioxide,

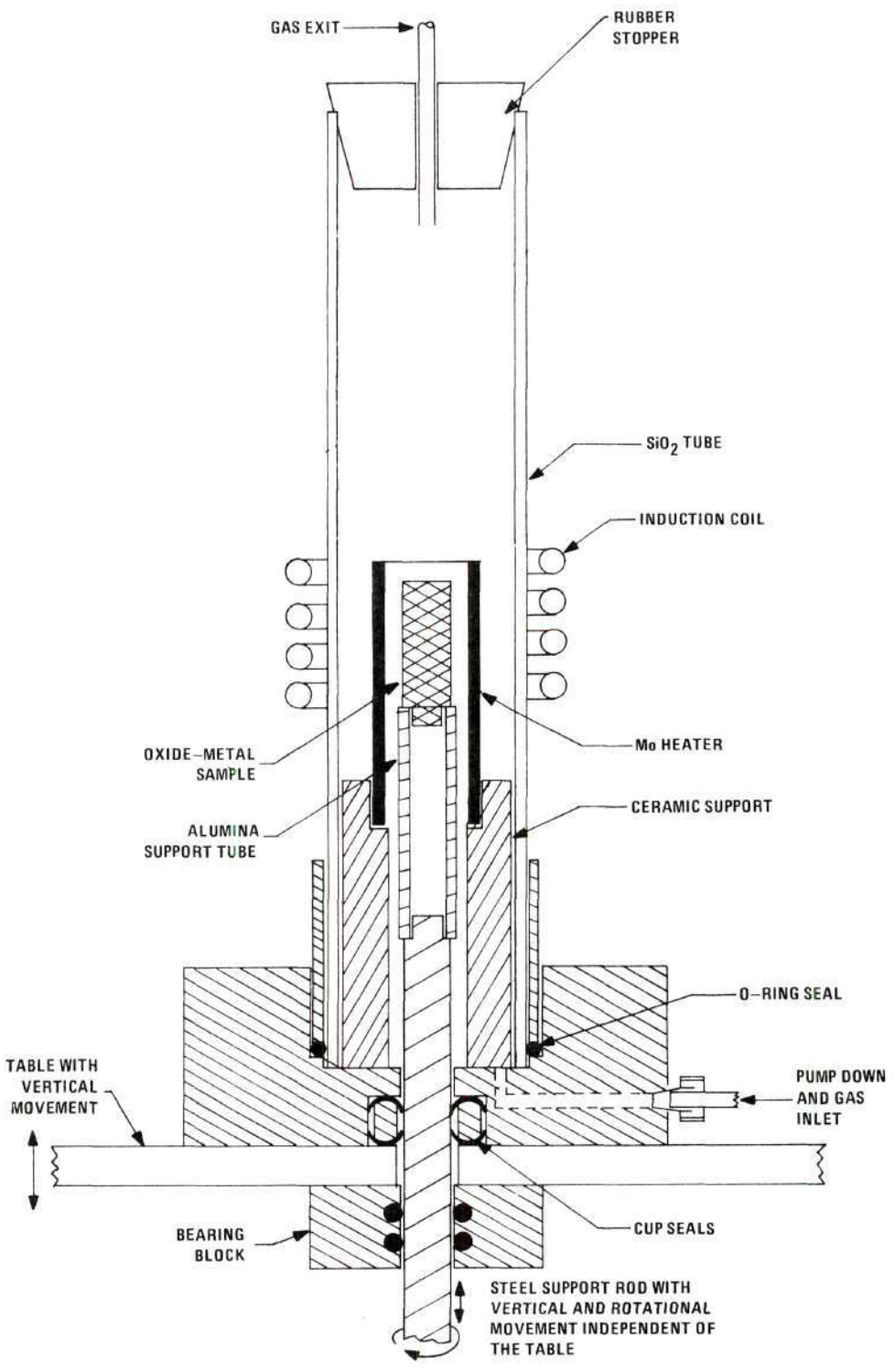


Figure 9. Diagram of the Induction Heating Facilities Showing The Position of The Molybdenum Suscepter when used as a Preheater

flow meters, and bubble bottles. The vacuum pump was used to evacuate the system to about 150 millitorr and to check for major leaks. The gases to be used passed through flow meters and entered the silica tube through the brass base. After exiting the silica tube at the top, the gas passed through a filter to trap airborne solids which would foil the vacuum shut off valve. The gas finally went through bubble bottles which prevented back streaming of any air into the system.

Analysis of exit gases was accomplished using a Carle, Model 8500, Basic Gas Chromatograph.

## Sample Preparation Apparatus

To increase the electrical conductivity of the samples, the uniaxially-pressed $UO_2$-W pellets were densified by sintering in a Harrop Model P-16-4-6 platinum heating element tube furnace. That furnace, incorporating a 9.21 cm inside diameter $Al_2O_3$ muffle, is capable of heating samples to 1600°C along its 15.25 cm hot zone.

## Examination of Samples

Microscopic examination of solidified samples was done using a Reichert Metallograph, which permitted both light- and dark-field observation over a wide range of magnifications.

# CHAPTER IV

## MATERIALS AND PROCEDURE

This chapter outlines the procurement and preparation of the $UO_2$ and W powders used as raw materials in the production of oxide-metal composites. Particular emphasis is placed on the formation of sample pellets and the subsequent growth procedure. A review of analytical techniques is also presented.

Due to the necessity of procedural variation in the optimization of composite growth, the following may be characterized as an "average" or "standard" procedure. Changes made during experimentation will be noted in the discussion of results.

### Raw Materials

The tungsten metal powder used was a 99.9% purity batch obtained from Teledyne Wah Chang. Uranium dioxide powders were obtained from the Nuclear Materials Corporation (NUMEC), Exxon Nuclear Corporation, Babcock & Wilcox, and Nuclear Fuel Services. All had greater than 99.9% purity (Appendix A). The oxygen-to-uranium ratios of the as-received powders were 2.270, 2.111, 2.104, and 2.160, respectively. All powders consisted of granules less than 40 micrometers in cross-section, except the Exxon powder, which was composed mostly of 2 to 3 mm lumps. Scanning electron microscopy showed these to merely be agglomerates of smaller particles.

A powder characterization study was conducted to evaluate the

several urania samples received. That study is discussed in Appendix A.

## Procedure

### Powder Preparation

Three kilogram batches of $UO_2$ were placed in a quartz-glass tube and heated to 600°C for 12 hours in a hydrogen atmosphere flowing at a rate of 300 cc/minute. This process reduced the oxygen-to-uranium ratio (O/U) of the powder to 2.00, and visibly disintegrated the flocs of particles. After cooling to room temperature in the reducing atmosphere, the powder was quenched by dumping it into and mixing it with granulated dry ice. By the time the dry ice had sublimed, the O/U ratio of the powder had risen to and stabilized at 2.04 to 2.07, depending on the moisture content, where the lower number was characteristic of a low moisture content powder. Uranium dioxide powders were stored in glass jars at room temperature until needed without appreciable stoichiometry changes.

### Sample Production

For reasons of cost and availability, all experiment runs used either NUMEC or Exxon powders, as noted in Appendix A. Two hundred thirty-five grams of $UO_{2.04-2.07}$ and 15 grams of W were weighed on an Ohaus triple-beam balance and hand-agitated to facilitate mixing. This $UO_2$-6 w/o W powder was then uniaxially pressed in a 3.2 cm die under a 15,000 pound load, crushed, and repressed at 7500 pounds. The result was a 3.2 cm diameter, 6.8 cm tall pellet, having an unfired (green) density of $4.60 \pm 0.10$ grams/cc.

Sample pellets were sintered in nitrogen flowing at 300 cc/minute

to increase the density, thereby increasing the electrical conductivity. A 24-hour cycle programmed on the automatic furnace controller heated the samples from room temperature to 1400°C in eight hours. A soak period of four hours was followed by a twelve hour cooling stage. At approximately 650°C, the heat loss from the furnace was insufficient to allow the program to be followed, extending the total firing cycle to 36 hours. The fired $UO_2$-W pellets were typically 6.0±0.2 cm tall, 2.5± 0.1 cm in diameter, and had densities ranging from 8.5 to 10.5 g/cc.

Composite Growth

The setup for the growth runs is shown in Figure 9. The pellet was centered within the coil on an alumina support. The molybdenum susceptor was placed concentrically around the pellet on its foam silica holder. A 50.8 cm long, 5.56 cm inside diameter silica glass tube was placed around the pellet and susceptor assembly for atmosphere containment. Care was required to properly center the pellet, susceptor, and silica tube within the load coil to prevent arcing upon the application of high power levels. After the sealing and evacuation of the system, a dynamic atmosphere of nitrogen flowing at about 400 cc/min was introduced. Rf power was then applied and gradually increased by an automatic controller over a period of about one hour, until the susceptor was heated to about 1300-1500°C. It should be noted that all temperatures cited are approximate, due to the fact that corrections were not made for emissivity, or radiation losses through the silica tube or the frequently-seen vapor deposits on the tube wall.

Once preheated, the sample had a sufficient electrical conductivity

for direct internal melting using rf induction heating. The coupling operation was the most difficult aspect of the procedure, as the time taken and the errors involved had to be held to a minimum. The power had to be reduced to prevent arcing as the susceptor was lowered out of the coil, and then, full power had to be applied before the sampled cooled substantially. If this was all done properly, direct rf heating occurred, and a stable molten zone was established within the pellet by balancing the power absorption and radiative heat losses at the surface. The surface temperature was held at about 1800°C by maintaining the rf generator at a 1.0 ampere plate current, and at about a 5.0 kilovolt plate voltage. After melting the nitrogen preheat atmosphere was replaced by one consisting of 99 v/o carbon monoxide and 1 v/o carbon dioxide, flowing at the same rate. The molybdenum susceptor was slowly raised into the bottom two turns of the coil, where it acted as a post-heater, and molten-zone cutoff point.

Composite growth was accomplished by lowering the pellet through the coil by controlled movement of a hydraulic cylinder. As the translation proceeded, material was melted from the top of the pellet, and solidified at the stationary front imposed by the post-heater susceptor. Once the pellet had lowered almost entirely into the susceptor, translation was stopped, the nitrogen atmosphere resumed, and a four-hour, automatic, slow-cooling period was begun.

Examination

After growth, most samples were sectioned longitudinally and/or transversely with a diamond saw. The sections were then ground with silicon carbide paper, and polished with 1μm diamond paste on a nylon

cloth. Macroscopic examination was done to establish size and shape of the solidified zone, cell structure, and overall appearance of the pellet. The polished sections were then microscopically examined to determine the fiber morphology.

# CHAPTER V

## RESULTS AND DISCUSSION

This chapter describes the parameters studied in an effort to optimize the routine melt-growth of $UO_2$-W composites using unidirectional solidification. Although an effort was made to divide these parameters into the subtopics listed in Table 2, it should be noted that most of these parameters are interrelated and affect each other. In addition, the effects of these parameters on fiber array uniformity and cracking characteristics are discussed.

Table 2. Parameters Controlling the Melt-Growth of $UO_2$-W Composites

1. Sample Size
2. Starting Oxide-Metal Composition
3. Solidification Atmosphere
4. Sintering Atmosphere and Pre-Melt Ingot Density
5. Solidification Rate
6. Molten Zone Control

Prior to discussing the experimental results in detail, it would be beneficial to briefly describe the "state of the art" in the unidirectional solidification of eutectic structures in the $UO_2$-W systems which existed before this work was begun. The basic growth technique remains the same as described in the experimental approach section of this thesis, and has not basically changed as a result of this work. Prior to

initiating this study, the critical influence of oxide stoichiometry on tungsten solubility in molten urania was recognized. The major problem for the routine and optimum growth of $UO_2$-W may be summarized as follows: for uniform fiber arrays to be grown for long lengths, it is necessary to obtain and maintain a homogeneous dispersion of the metal molecules or atoms in the molten zone. It was seen, in the early work, that the solidified oxide-metal composites typically contain less metal than originally used in the starting mixture. Consequently, any reproducible and satisfactory growth scheme must contend with the continual depletion of the metal from the molten zone, predominantly through some type of vaporization or oxidation process. In the case of $UO_2$, this process is complicated by the need to maintain the stoichiometry of the molten oxide above 2.00, since the increased oxygen potential required to satisfy this requirement aggravates the tungsten oxidation and vaporization problems. In addition, any modification of the growth scheme designed to maintain steady state and uniform conditions during solidification requires that the system be maintained at temperatures in the neighborhood of 2800°C, where oxidation and vaporization reactions proceed very rapidly. Because of these problems, prior to this work most of the successful growth was limited to lengths only slightly greater than one centimeter, primarily because of the depletion of the tungsten from the molten zone. The decision was made at the outset of this work to attempt to increase the size of the starting samples, or ingots, in an effort to both grow larger areas of fiber array, and to decrease the rate of metal loss by increasing the mass-to-surface area ratio of the molten material. Since that change was beneficial to the successful growth of the increased-

size ingots, it will be the first topic to be discussed in this chapter.

The parameters and results of the various growth runs are tabulated in Appendix B. Smaller, more specific tables will be included in the discussion for convenience.

## Sample Size and Fiber Array Uniformity

Experiments in previous studies (3-5, 7-10, 12,14,21, 26-29) as well as preliminary runs conducted during this investigation, have utilized sample pellets with unfired (green) diameters of 19 mm, and sintered diameters of about 16 mm.

Since the kinetic reactions associated with the very high temperatures required to grow $UO_2$-W composites cannot be avoided, the decision was made to increase the diameter of the ingots in order to increase the mass of molten material compared to the surface area, thus decreasing the rate of composition change in the liquid. Transverse sections of the three different ingot diameters are shown in Figure 10. The smallest wafer (16 mm diameter) is typical of the $UO_2$-W samples solidified prior to this study, while the intermediate (25 mm) and large diameter (32 mm) wafers are from experiments LBH-15A and LBH-11, respectively, which were performed during this research.

Preliminary runs indicated that with minor adjustments to existing equipment, including decreasing the frequency from 3.7 to 3.4 megahertz, sintered intermediate size ingots 25 mm in diameter (32 mm green) could be easily melted and resolidified. The most encouraging feature was the significantly larger cell sizes present in the samples. That improvement is probably attributable to the wide and flatter liquid-solid inter-

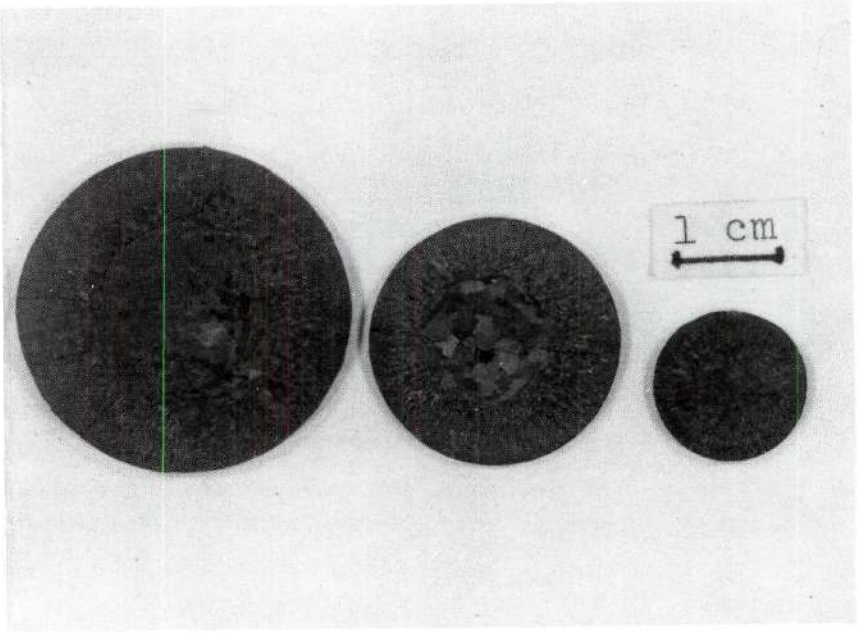


Figure 10. Transverse Sections of 16, 25, and 32 Millimeter Diameter $UO_2$-W Samples

face present in the larger samples. Evaluation of those samples revealed that the uniformity of the fiber geometries was also greatly improved over the smaller samples, providing substantial areas of uniform composite for the production of emitter arrays.

Evaluation of fiber geometry uniformity of the small (16 mm) diameter ingots revealed that the transverse fiber density of $UO_2$-W composites varied less than $\pm$10% within several millimeters of the center of the solidified zone. That value increased to $\pm$20% as the distance from the center increased, and at the edge, very large variations in density were observed. It was also noted that fiber density generally decreased from the base to the top of the solidified zone. Variations in fiber densities of the 25 mm diameter samples followed approximately the same trends as had been seen previously in the smaller pellets, but were reduced by about one half.

A typical 25 mm diameter ingot, having a composition of $UO_{2.07}$-6 w/o W, which was grown at 2.8 cm/hr, was sectioned at three levels in the solidified zone. Central and circumferential areas of each wafer were examined using a scanning electron microscope. Representative pin diameters were measured from SEM photographs of those samples. The results are in Table 3, below, along with fiber densities, as determined from optical micrographs.

These results indicate that the fiber diameter generally increased with decreasing fiber density at both the centers and the edges of the wafers. Based on this limited data, there is no apparent trend in the relationship between center and edge pin diameters. A typical area of

Table 3. Analysis of W Fiber Densities and Diameters From Selected Locations in Sample Number LBH-5A

| Slice Number | Level From Bottom of Zone (mm) | Fiber Density ($10^6$ pins/cm$^2$) center | edge | Fiber Diameter (μm) center | edge |
|---|---|---|---|---|---|
| 4 | 4 | 13.0 | 11.4 | 0.35 | 0.44 |
| 5 | 9 | 12.1 | 10.0 | 0.43 | 0.44 |
| 8 | 30 | 9.8 | 6.3 | 0.47 | 0.58 |

uniform fiber growth is shown in Figure 11.

Further sample-size experiments (LBH-11, 12) showed that low density tungsten fiber geometries can also be grown in $UO_2$-W ingots that are approximately 32 mm in diameter when sintered. There are, however, some problems associated with the unidirectional solidification of larger ingots: analysis of the shape of the solidified zone and associated void in those samples suggested that there were substantial heat losses from the top of the sample, and that the rf power penetration depth was insufficient to completely melt the center. In an effort to overcome those problems, the circuitry of the Lepel rf generator was modified to decrease the frequency to improve power penetration, but only a small change could be made (from 3.4 to 3.1 MHz) without adversely affecting the efficiency of the generator. A large diameter $UO_2$-W ingot was fabricated using the procedures previously reported. An insulating cap was fabricated from a high-$Al_2O_3$ fibrous material to decrease the heat loss and help flatten the solidification front. Toward the end of this growth experiment, the surface temperature of the top of the ingot ex-

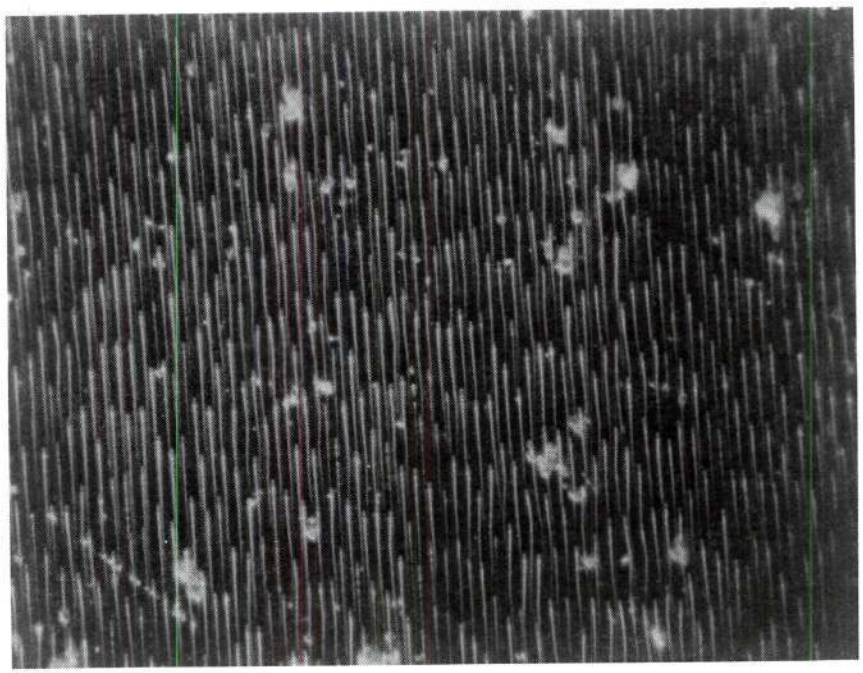

Figure 11. Typical Area of $UO_2$-W Composite Growth 542x,dark field

ceeded 1700°C (maximum use temperature of the fiber insulator) and the insulator melted and/or reacted with the sample. Analysis of the composite structure after solidification indicated both of these changes help flatten the liquid-solid interface and improve the composite geometry.

Because of the problems associated with the use of such large pellets, including materials utilization (500 grams per run versus 250 grams for the 25 mm diameter pellets), the 25 mm diameter sample size was chosen for most runs. It appears likely however, that uniform growth could be accomplished in the 32 mm pellets if taller pellets were used, to limit heat losses from the ends.

While the utilization of the larger diameter $UO_2$-W ingots yielded improved eutectic geometries of increased size, it also required isothermal sintering of the ingots prior to internal melting and resolidification. That requirement necessitated an investigation of stoichiometry changes and densification during sintering as a parameter controlling the growth of $UO_2$-W composites. Those areas are covered in later sections of this chapter.

Having established the ingot size for use with the equipment available this investigation was directed toward the effect of oxide-metal composition on fiber geometries of the composite.

## Oxide-Metal Composition

Past studies (8,30) indicated that the unidirectional solidification of 16 mm diameter ingots having a composition consisting of urania with an O/U of 2.04 and 6 w/o tungsten yielded uniform fiber geometries

ranging from 10 to 30 million fibers per square centimeter. During some of those experiments, it was noted that uniform fiber growth was obtained for only short lengths before changing into degenerate morphologies unusable for the production of emitter arrays.

During this investigation, the unidirectional solidification of 25 mm diameter samples with that composition typically yielded fiber densities from 5 to 30 million fibers per square centimeter for growth periods substantially longer than had been achieved previously. Due to the extensive, uniform growth obtained with that composition in the intermediate-sized samples, no further changes in oxide-metal composition were made.

The influence of solidification (growth) atmosphere on the characteristics of $UO_2$-W composites is discussed in the following section.

## Solidification Atmosphere

A series of $UO_2$-W growth experiments was run holding all parameters as constant as possible except for variation of the growth atmospheres. Studies of pure urania (25) indicate that at melting temperatures, a CO-1 v/o $CO_2$ atmosphere yields an O/U ratio near 2.03, and since tungsten solubility (22) is substantial at that O/U ratio, the atmospheres tested were designed to provide oxygen potentials that would establish O/U ratios near 2.03. Solidification was accomplished using the following gas mixtures: $H_2$ saturated with $H_2O$; CO + 0.1 v/o $CO_2$; CO + 1.0 v/o $CO_2$; and lastly, CO + 4 v/o $CO_2$. In all of these runs a well-developed uniform molten zone was achieved, and analysis of the resultant structures showed substantial variations in composite growth

characteristics. Fiber density measurements made along the longitudinal growth directions of these samples yielded a range of fiber densities between 5 and 30 million pins per square centimeter. A general improvement of fiber array uniformity was observed with decreasing oxygen pressures. In all samples, there appeared to be a continual decrease in fiber density from the base to the top of the solidified region.

Another group of experiments were performed where inlet and exhaust gases were monitored using a gas chromatograph. In $UO_2$-W solidification experiments where the inlet gas consisted of CO with 0.1 v/o $CO_2$, the exit gas composition showed an extremely high concentration of $CO_2$ (8-10 v/o) during the initial melting. During the period of growth (approximately 90 minutes), the $CO_2$ content slowly decreased and eventually stabilized at 0.3 v/o.

An experiment was run to ascertain the O/U ratio obtained when a pure $UO_{2.04}$ sample was melted and held until the exit gas reached the CO-0.3 v/o $CO_2$ composition. Post-melting analysis showed the O/U ratio to be 2.023. In an additional experiment, the Mo pre-heater was run at approximately 1400°C without any oxide-metal mixture in the $CO_2$-0.1 v/o $CO_2$ mixture, and again the equilibrium concentration of $CO_2$ was found to be about 0.3 v/o. This behavior suggests the reaction, $2CO \rightarrow C + CO_2$, occurred in the system. Conclusive evidence for this reaction was the presence of carbon black found on samples and support fixtures. Similar samples, grown in a CO-1.0 v/o $CO_2$ atmosphere, displayed a similar pattern in reaching an equilibrium $CO_2$ concentration of about 1.2 v/o.

The atmosphere consisting of carbon monoxide with 1.0 v/o carbon dioxide was selected for use in most experiments because the oxygen po-

tential it provided facilitated an O/U ratio in urania which permitted reasonable tungsten solubility in the melt, as previously stated in the urania section of the Literature Survey.

Having established the size and metal content of the sample ingots, and the atmosphere used during the growth procedure, an appreciation of the effects of the O/U ratio of the oxide, as determined by sintering atmosphere, as well as the bulk density of the pellets, was developed. A discussion of these parameters followed.

## Sintering Atmosphere and Premelting Ingot Density

In an attempt to evaluate the role of the pre-growth sintering conditions on the growth of $UO_2$-W composites and the characteristics of the resulting material, a series of experiments was performed in which reducing, neutral, and oxidizing atmospheres were utilized during the sintering of samples LBH-16, 18, 19, respectively, the starting compositions of all samples was urania with an oxygen-to-uranium (O/U) ratio of 2.07 mixed with 6 w/o tungsten metal. Included with each pellet during sintering was a smaller $UO_2$-W pellet for the purpose of establishing the post-sinter, pre-growth microstructure of the pellets, and a pure $UO_2$ pellet for evaluating the resultant O/U ratio. Green densities of the as-pressed oxide-metal pellets were $4.65 \pm 0.05$ g/cc. All samples were sintered at 1400°C for four hours during a 36-hour total firing cycle. The sintering parameters and associated properties are listed in Table 4.

The reducing atmosphere used in experiment LBH-16 consisted of 250 cc/min $N_2$ plus 50 cc/min $H_2$. The sample pellet had a fired density

Table 4. Atmospheres Used, and Resulting Properties Of Samples Used in Sintering Study

| Sample | Sintering Atmosphere(cc/min) | Fired Density(g/cc) | Fired O/U Ratio |
|---|---|---|---|
| LBH-16 | $N_2$:250, $H_2$:50 | 8.83 | 2.00 |
| LBH-18 | $N_2$:300 | 9.77 | 2.01 |
| LBH-19 | $CO_2$:300 | 9.17 | 2.10 |

of 8.83 g/cc, an O/U ratio of 2.00, and the tungsten appeared as elemental metal particles in the grainy oxide matrix (Figure 12). Microstructural examination revealed flattened pores and grain boundaries that were uniaxially pressed. After unidirectional solidification in a manner known to produce uniform, low density fiber geometries using a CO-1 v/o $CO_2$ atmosphere, the pellet was longitudinally sectioned. A reasonably well-developed solidified zone was present (Figure 13), but no metal fibers were found and most of the W appeared as metal droplets frequently associated with pores. This behavior was as expected, since tungsten solubility is very limited in molten urania with an O/U ratio near 2.00. During the solidification phase of experiment LBH-16, analysis of the exit gases using a gas chromatograph showed a decrease in $CO_2$ content from the inlet analysis of 1.0 v/o to about 0.15 v/o, indicating that the sample absorbed oxygen from the atmosphere. The volume of $CO_2$ gradually increased to about 0.95 v/o at the end of the run.

Nitrogen following at 300 cc/min was the "neutral" atmospheres used in LBH-18, which yielded a sintered oxide-metal sample with a density of 9.77 g/cc, and an O/U ratio of 2.01. Microscopic observation

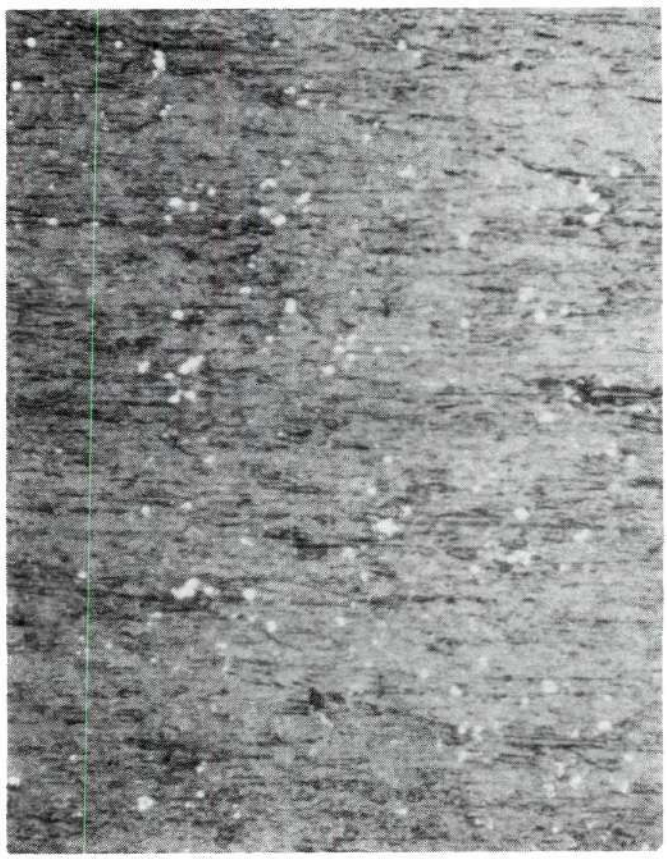

Figure 12. Photomicrograph of $UO_2$-W Sample Sintered in a Reducing Atmosphere ($H_2/N_2$) Showing Elemental Metal and Oriented Oxide Grains 196X

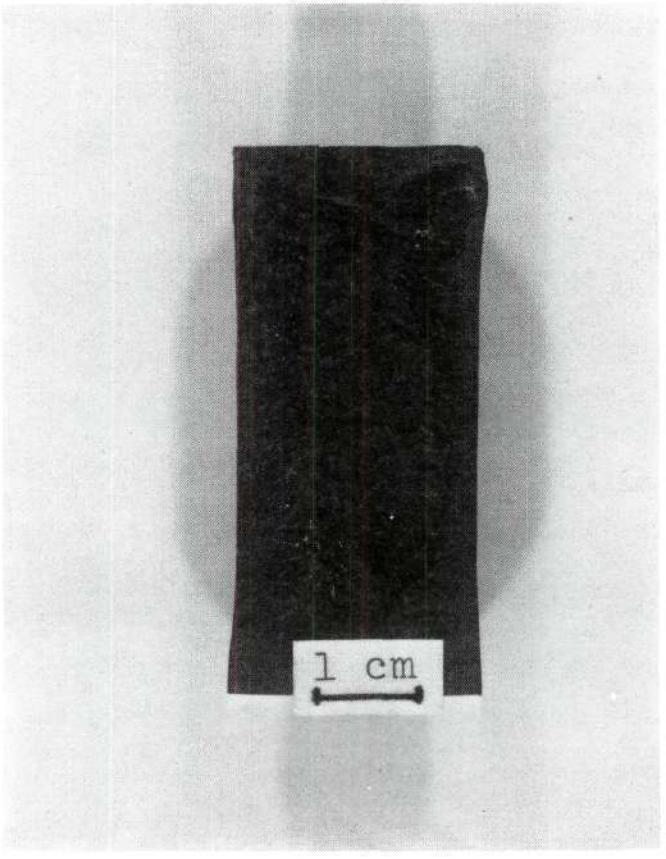


Figure 13. Post-Run Longitudinal Section of $UO_2$-W Sample Sintered in a Reducing Atmosphere,(LBH-16)

(Figure 14) showed that the pellet consisted of $UO_2$ with no particular grain boundary or pore orientation. The tungsten was present as rounded metal particles often surrounded by a "blue" phase (with an approximate formula of $U_xUO_3$). This phase was frequently seen in the cell boundaries of the composite samples after solidification.

After unidirectional solidification of LBH-18 in the standard manner, extensive areas of "good" fiber growth were observed with a few small areas of the "blue" phase in the grain (cell) boundaries.

A gas chromatograph trace of the exit gas analysis during experiment LBH-18 showed an instantaneous rapid outgassing of oxygen as reflected by the high $CO_2$ content of the atmosphere upon melting. The presence of $CO_2$ in excess of the inlet volume slowly decreased to a final value of about 1.3 v/o, reached near the end of that experiment.

An oxidizing atmosphere consisting of $CO_2$ flowing at 300 cc/min was used during the sintering of the $UO_2$-W pellet during experiment LBH-19. After sintering, the O/U ratio was 2.10, and the pellet appeared grainy and porous (Figure 15) and had a density of 9.17 g/cc. During solidification in the standard CO-1 v/o $CO_2$ atmosphere, extreme outgassing by the pellet and fogging of the atmosphere-containment tube occurred, and it was not until the end of the run that it was discovered that the pellet had expanded and stuck in the molybdenum post-heater. Because of this difficulty, molten zone travel was limited to approximately 1 cm (Figure 16). However, after two hours of stationary melting, there was still enough metal dissolved in the molten oxide to produce fibers as the melt solidified during cooling. This behavior may indicate that a higher O/U ratio may help during the growth of long lengths of continuous

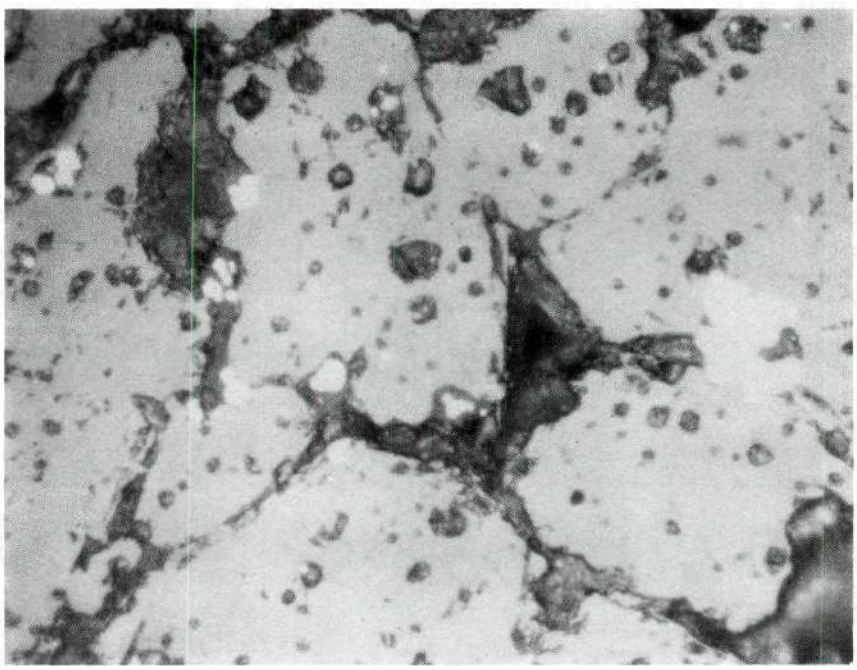

Figure 14. Sample Pellet Sintered in a Neutral Atmosphere ($N_2$) Showing Rounded Metal Particles Surrounded by "Blue Phase" 542X

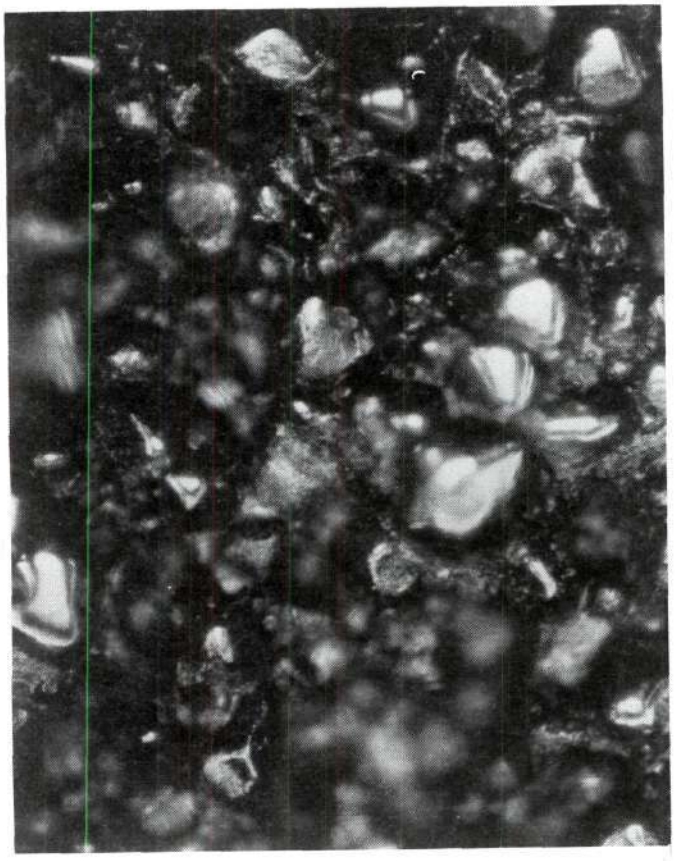

Figure 15. Sample Pellet Sintered in an Oxidizing Atmosphere ($CO_2$) Showing Extreme Graininess and Porosity 196X

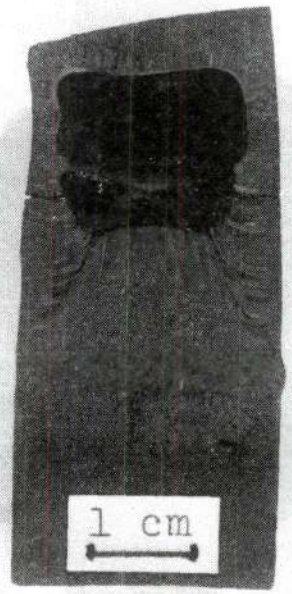


Figure 16. Sample LBH-19 After Growth Run Showing Area of Good Growth at Top of Solidified Zone

W fibers.

Exit gas analysis during experiment LBH-19 showed a very high volume of $CO_2$ initially, decreasing to about 3 v/o during the two and one-half hour run. That behavior indicated a rapid outgassing of oxygen from the sample throughout the experiment.

Experiment LBH-5, using a sample with a particularly high O/U ratio (2.20) and a corresponding increase in metal content (12 w/o), was designed specifically in an attempt to grow long lengths of continuous fibers. During melting, a very irregular, unstable zone was formed, and post solidification examination (Figure 17) revealed that the interior of the rod was poorly melted, suggesting a non-homogeneous oxide-metal liquid. This information indicates an upper-limit to useful O/U ratios near 2.10.

The role of pre-melting sample pellet density on $UO_2$-W composite growth characteristics was another aspect of this investigation. To assess that role, three pellets were fabricated using a composition known to produce good growth ($UO_{2.07}$-6 w/o W). The densities were controlled by varying pressing procedures, as listed in Table 5. The pellets were pressed in a 32 mm diameter die, and sintered in a $N_2$ atmosphere at 1400°C for four hours. The three pellets were melted and unidirectionally solidified using the same power setting, growth rate, and atmosphere, in accordance with established growth procedure.

Samples LBH-8A and LBH-8B displayed double voids (Figure 18) upon longitudinal sectioning, while LBH-8C, the sample of highest density, showed an area of poorly-melted material in place of the second void. No tungsten fiber growth was present in the lowest density sample, while


Figure 17. Post-Run Longitudinal Section of LBH-5, Showing the Lack of Establishment of a Stable Molten Zone

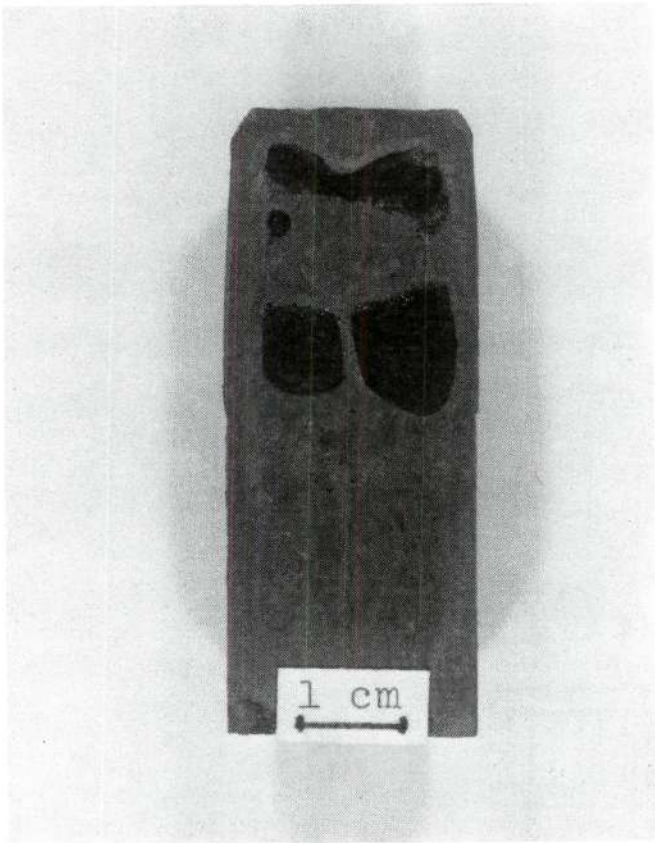


Figure 18. Sample LBH-8B, Showing Double Void

Table 5. Pellet Fabrication Data for $UO_2$-W Samples LBH-8A,B, and C

| Sample | Prepressing Load (lbs) | Final Pressing Load (lbs) | Green Density ($g/cm^3$) | Sintered Density ($g/cm^3$) |
|---|---|---|---|---|
| LBH-8A | 4000 | 2500 | 4.16 | 8.01 |
| LBH-8B | 4000 | 5000 | 4.43 | 8.83 |
| LBH-8C | 4000 | 7500 | 4.60 | 8.55 |

the intermediately-dense pellet displayed irregular fiber arrays in the area between the two voids. The most dense sample (LBH-8C) showed very uniform, low fiber density growth above, below, and on either side of the poorly melted segment of the molten zone. Note, however, that the pre-melting, sintered densities were 0.5 to 2.0 g/cc lower than those of most other sample pellets utilized for composite growth (cf Appendix B). These data suggest the influence of pre-melting density on the shape of the molten zone is more significant than anticipated. For a composition of $UO_{2.07}$-6 w/o W, the effective lower density limit appears to be about 8.5 $g/cm^3$ or about 75% of theoretical density.

The parameters discussed thus far have dealt with conditions imposed during the fabrication of sample ingots. The following section, covering solidification or growth rate, begins evaluation of changes made during melting and solidification.

## Solidification Rate

The influence of solidification or growth rate on composite structures formed during unidirectional solidification has shown (3-5,8) a

definite correlation: a decrease in growth rate led to a decrease in fiber density and a simultaneous increase in fiber size. Although no sample series were run to verify that behavior it was utilized successfully in the following examples: Since theoretical analysis (8,31) of the field emission performance of multi-pin arrays suggests that lowering the pin densities of emitter samples should help to improve electron emission capability, two experimental $UO_2$-W growth runs were made utilizing procedures specifically designed to decrease fiber density. Pertinent information is listed in Table 6.

Table 6. Composite Growth Parameters of Experimental Samples LBH-20, and LBH-21

| Sample | Starting o/u | Composition W Content(w/o) | Post-sinter o/u | Post-sinter Den.(g/cc) | Solidifi. Rate (cm/hr) | Avg. Fiber Density ($10^6$pins/cm$^2$) |
|---|---|---|---|---|---|---|
| LBH-20 | 2.07 | 6 | 2.01 | 10.30 | 1.50 | 5.0 |
| LBH-21 | 2.07 | 6 | 2.01 | 9.87 | 0.50 | 1.6 |

Experiments LBH-20 and -21 consisted of $UO_{2.07}$-6 w/o W samples that were sintered in a nitrogen atmosphere to densities of 10.30 and 9.87 g/cc, respectively. The preheating of the samples prior to unidirectional solidification was conducted in the usual manner utilizing a nitrogen atmosphere. After internal melting, the growth procedure was modified to reduce the fiber density: in LBH-20, the growth atmosphere was changed from the "standard" CO-1 v/o $CO_2$ to CO-0.5 v/o $CO_2$ in order to lower the oxygen potential. Lowering the equilibrium O/U ratio of

the molten urania has been shown (8,13,22,26,30) to decrease the amount of dissolved metal available for precipitation into ordered fiber geometries. The growth rate during LBH-20 was also lowered from the usual 3.0 to 1.5 cm/hr to further reduce the tungsten pin density. Post-run analysis of the sample, using photomicrographs of transverse sections revealed in Figure 19 an area in the center of each composite wafer characterized by uniform fiber geometries with densities ranging from 3 to 5 x $10^6$ fibers per square centimeter. Cracking in the center was limited to intergranular fissures, but the grains were large enough to permit the fabrication of single-cell emitter samples up to about 4 mm in diameter.

Since, compared with previous runs, it was possible to make a significant reduction in fiber density during Experiment LBH-20, the next experiment, LBH-21, was performed utilizing a further lowering of the growth rate to 0.5 cm/hr. Post-run analysis of this sample showed cracking characteristics and cell sizes similar to those in LBH-20, and the tungsten fiber densities were lowered to between 1.4 and 1.7 million fibers per square centimeter (Figure 20). Interestingly, the better fiber geometries were found in the upper portion of the ingot during this run, whereas just the opposite behavior was typical in the small diameter (16 mm) ingots. It had been anticipated prior to these experiments that the loss of W through various vaporization processes would restrict the solidification of uniform fiber geometries during long term, slow growth rate experiments.

Although the capability of reducing the pin density of cathode

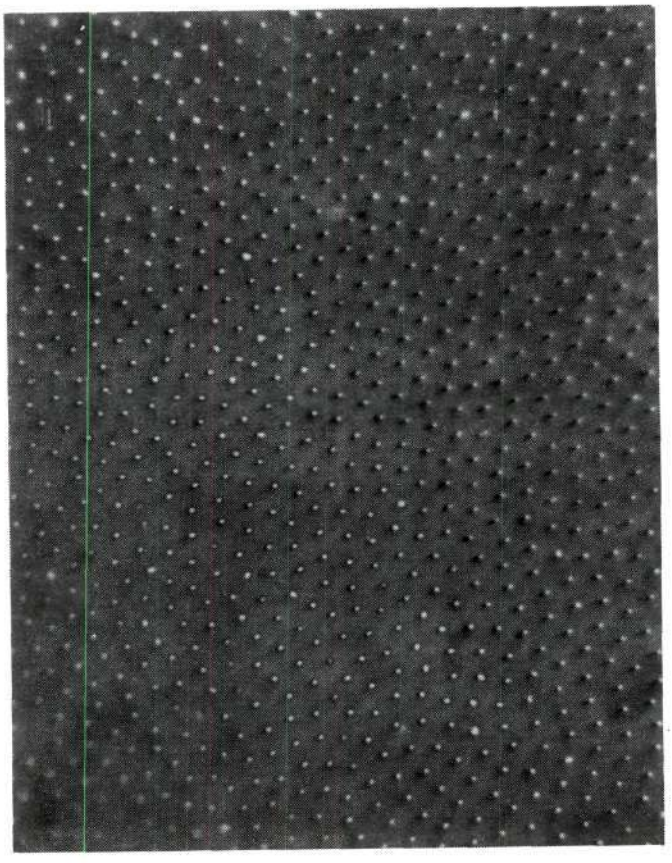

Figure 19. Photomicrograph of Transverse Section of Sample LBH-20 Showing Typical Tungsten Fibers 542X

(a)

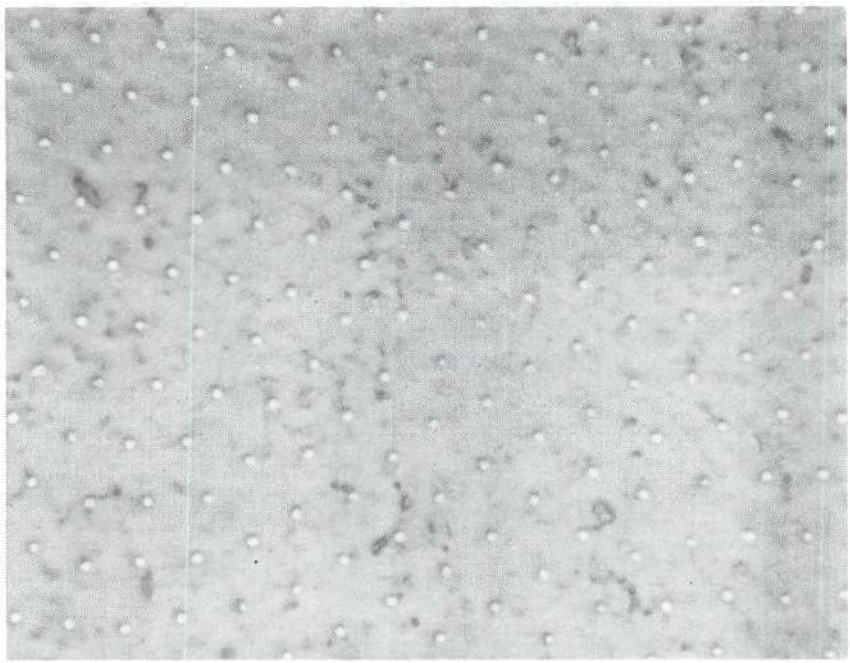

(b)

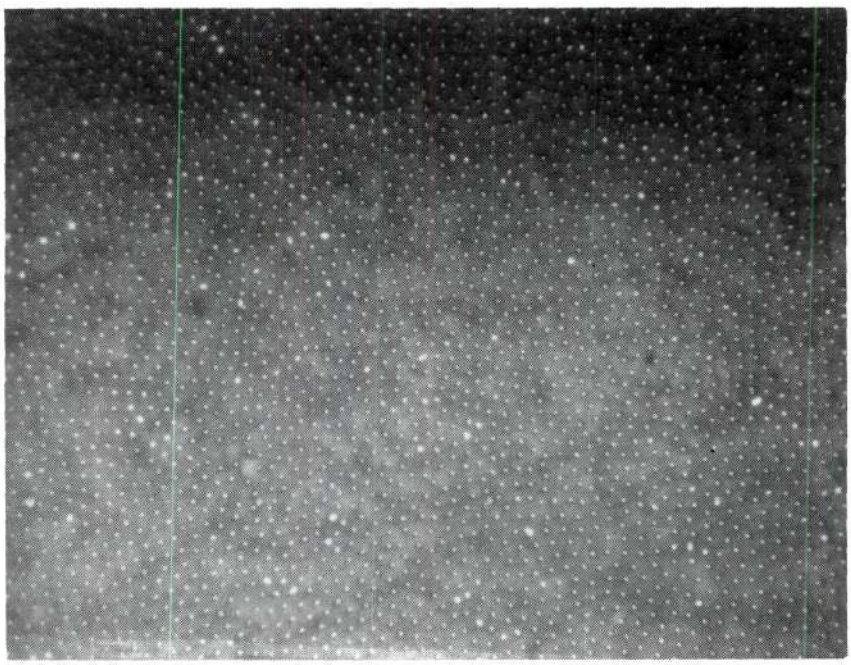

Figure 20. Transverse Section of (a) Sample LBH-21, Showing High Degree of Uniformity and Extremely Low Fiber Density ($1.6 \times 10^6$ pins/cm$^2$), 945X, and (b) Sample LBH-10A for Comparison ($31 \times 10^6$ pins/cm$^2$), 945X

samples by almost a factor of ten is significant it is still desireable to produce large, uniform areas of continuous fiber growth. Key factors in that consideration, are control of the size, shape, and translation of the molten zone within the sample ingot. Establishment and control of the molten zone is facilitated by the proper application of the induction-heating field, as discussed below.

## Molten Zone Control

Molten zones were easily established in most of the $UO_2$-W solidification experiments, tending to expand over the entire length of the pellets as the power was increased. A comparison of Experiments LBH-4 with LBH-15A lends insight into a general tendency observed during this study: The samples were of the same composition, had approximately the same densities, and were solidified at nearly the same growth rates. The power settings for LBH-15A were 8 percent greater than those employed in LBH-4. The increased power input caused the lengthening of the molten zone from about half of the pellet to about three-fourths, allowing the homogenization of a greater mass of material prior to solidification. Post-run sectioning revealed fiber densities very near to each other: 10 million fibers per square centimeter for LBH-4 versus 12 million for LBH-15A--a difference that may be attributed to the slight variation in growth rates. The fiber array uniformity, however, was much better in LBH-15A than in LBH-4. This, apparently, was due to the size stability of the solidified cells. In Figure 21, longitudinal sections of those samples, the difference can be seen: in LBH-4, many small cells were nucleated and solidified early in the run. Those gradually began to

(a)

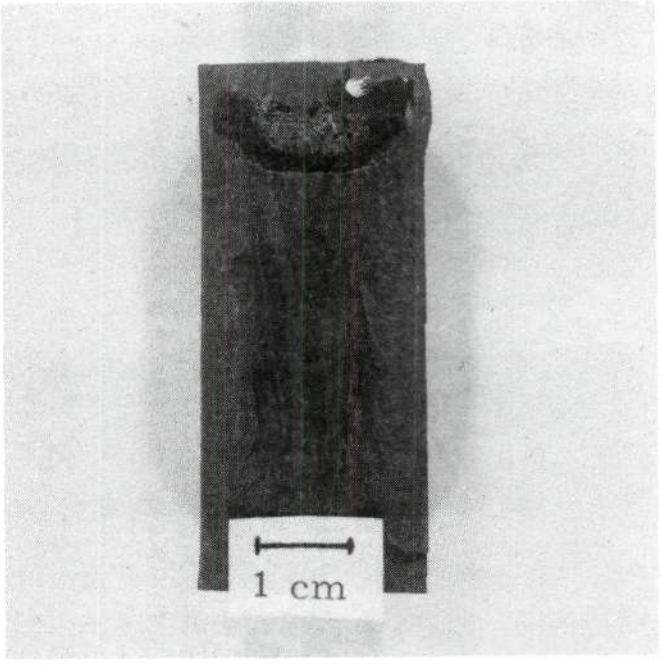


(b)

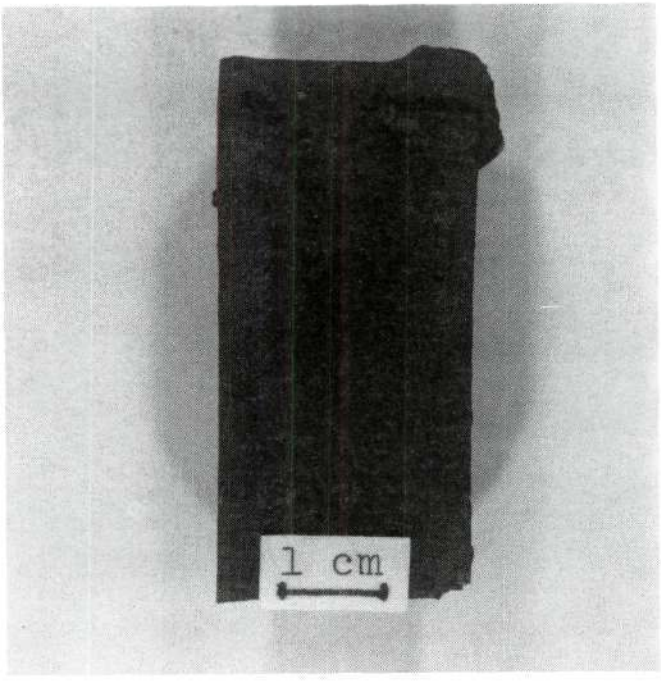


Figure 21. Longitudinal Sections of (a) LBH-4, and (b) LBH-15A, Showing Variation of Cell Size with Position in Sample

increase in size, with the associated decrease in number, until there were a few large cells, surrounded by smaller ones, at the top of the solidified zone. Sample LBH-15A, however, displayed the formation of larger cells relatively early in the solidification process, which remained more-or-less unaltered throughout the remainder of the run. The size-stability of the solidified cells was probably due to the creation of both a more homogeneous melt, and a flatter solidification front. Those factors are controlled by the power-penetration characteristics of the equipment.

The effective skin depth of the electric field (32) is partially determined by the geometry of the induction coil. As the ratio of the length of the coil to its diameter decreases, the penetration into the sample by the electric field also decreases. Consequently, a shorter coil leads to a smaller effective skin depth, which may eliminate power instabilities created by the temperature dependence of the electrical conductivity of the materials, but it may also adversely affect the shape of the molten zone and hence, the solidification front.

Samples LBH-1 through 8C were melted using a 6.67 cm inside diameter, 4 and 1/2 turn load coil. Those samples yielding fiber arrays typically displayed geometries with 5 to 25 million fibers per square centimeter. Cell sizes were typically on the order of 1 to 3 mm in cross-section. Samples LBH-9, 10A, 10B, and 13 through 21 were induction melted using a 5 and 1/2 turn coil--an increase of about 1.25 cm in height. There were no apparent instabilities created by the change in the coil geometry, and fiber densities realized were in the same range as before. The average cell size, however, was increased to an average

cross-section of 5 mm, evidently due to a flattening of the solidification front.

In order to produce uniform tungsten fiber geometries during the unidirectional solidification of $UO_2$-W ingots, it was necessary to establish a homogeneous zone of liquid in the samples prior to the initiation of the solidification process. This was accomplished during the initial internal melting by increasing the power input to the sample until the molten zone size had been maximized and stabilized. However, when the lower molybdenum susceptor was raised into the bottom of the rf work coil to serve as a postheater, and solidification-front cutoff point, the inductive field was drastically distorted. That apparently caused the solidification front to run upward in an uncontrolled fashion for a short distance, yielding numerous small cells and areas of primary $UO_2$ at the bottom of the zone, with the tungsten metal randomly precipitated as droplets. As the solidification front slowed and stabilized, the average cell size increased to approximately 5 mm in diameter, and very uniform, low-density fiber geometries were realized.

In an effort to eliminate this initial runaway situation, in experiment LBH-14, an upper molybdenum preheater was utilized in addition to the postheater to "pin" the molten zone in the 25 mm gap between the susceptors. Post-run analysis of that sample revealed the presence of many small cells, and few areas of continuous fiber growth. "Fan-banding," a situation apparently involving the repeated nucleation and extinction of fiber growth, was prominent throughout the solidified zone of that sample (Figure 22).

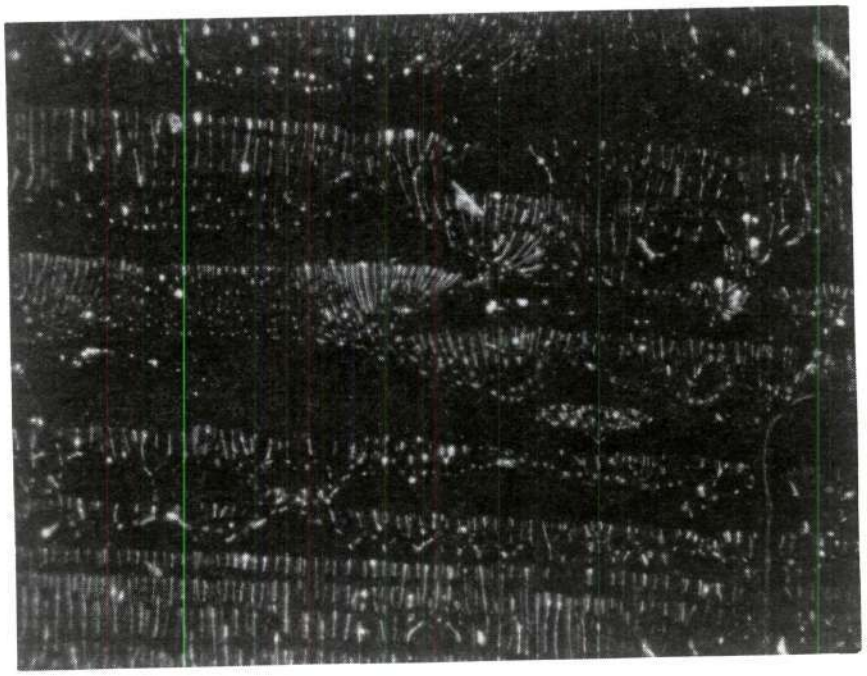

Figure 22. Typical Area of "Fan-Banding", Apparently Involving the Repeated Nucleation and Extinction of Fiber Growth. Sample LBH-14; dark field, 542X

The possibility that the discontinuous growth was due to a "sub-critical" size of the zone "pinned" between the susceptors led to experiment LBH-17, where the gap between the pre- and post-heaters was increased to 36 mm (from the 25 mm separation of LBH-14). Post-run analysis of LBH-17 revealed that the change had a minor effect on cell size, as the majority of cells were only slightly larger than those seen in LBH-14. The previously seen "fan-banding" was also present, but the average distance between the nucleation and extinction of fiber growth was substantially increased (Figure 23). Moreover, some cells were almost completely free of banding, and in some regions continuous fibers ran the entire length of the solidified zone. This general improvement in fiber growth suggests that this type banding may be related to the size of the molten zone.

It appears as though the two procedures offer their own advantages and disadvantages: the use of a single susceptor allows the establishment of a large, homogeneous molten zone, but is plagued by the initial runaway solidification front problem, as well as overheating as the molten-zone approaches the top of the pellet. The double-susceptor configuration offers more precise control over the translation of the molten zone, but does not provide for homogeneity. A third possibility, discussed in the next section, was developed to help alleviate cracking problems, but may also be a much-improved technique for molten-zone control: instead of lowering the pellet into the susceptor, the susceptor was slowly raised around the pellet, which helped alleviate the "runaway" condition.

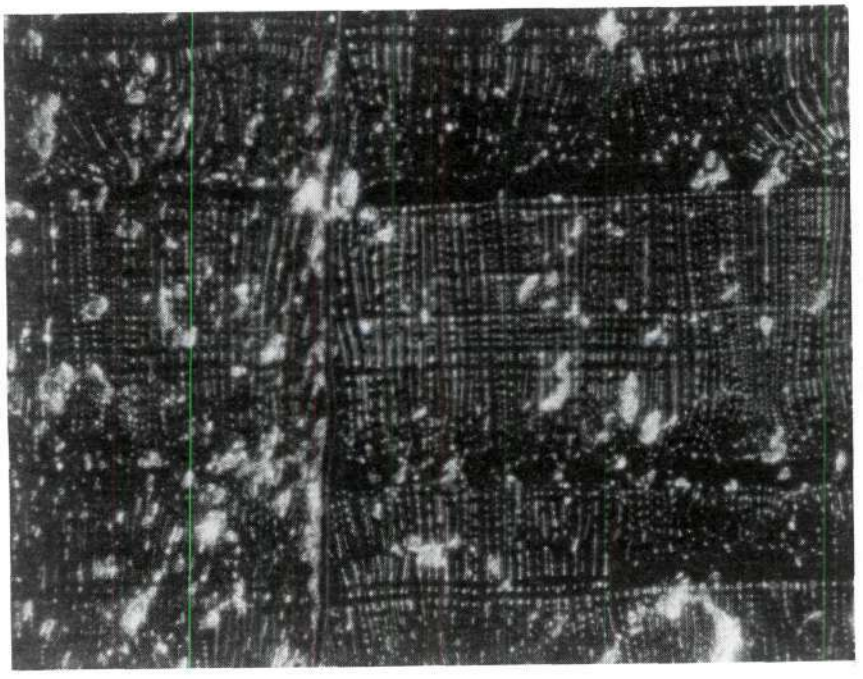

Figure 23. Typical Area of "Fan-Banding" From LBH-17
Showing General Improvement in Fiber Lengths dark field,542X

## Cracking Characteristics

Throughout the experimentation, cracking of the samples presented a problem critical to the utilization of these materials in the fabrication of cathode structures: Sample LBH-4 (Figure 21), displayed a single, large crack, along the right side of the solidified zone. Such fissures would hinder the production of large-area cathodes, as the tendency was for the crack to extend through the center of the sample, frequently causing transverse sections to break in half.

Increasing the size of the sample ingots from 16 to 25 to 32 mm in diameter provided larger usable areas of fiber growth, but did not appreciably alter the cracking characteristics. The cracking appeared to be due to the difference in contraction of the internal, solidified area, and the external, unmelted skin material during cooling. In an attempt to overcome that problem, four 5 mm deep, 0.03 mm wide vertical grooves were made with a diamond blade at 90° intervals down the entire length of sample pellet LBH-6 before melting. It was theorized that the gaps would provide room for the skin of the pellet to shrink without stressing the interior region. Cracking appeared to be less severe, but the shape and size of the molten zone was severely altered, especially near the gaps as can be seen in Figure 24. In a second experiment, LBH-9, the number of gaps was increased to eight. These grooves had the same cross-sectional area, but were wider than before, being 1 mm wide by a tapering 0.3 mm deep, as cut by a dental burr. Post-solidification analysis of that run revealed that the major cracking occurred circumferentially, about two-thirds of the way from the center to the edge of the solidified zone. The zone shape was improved by

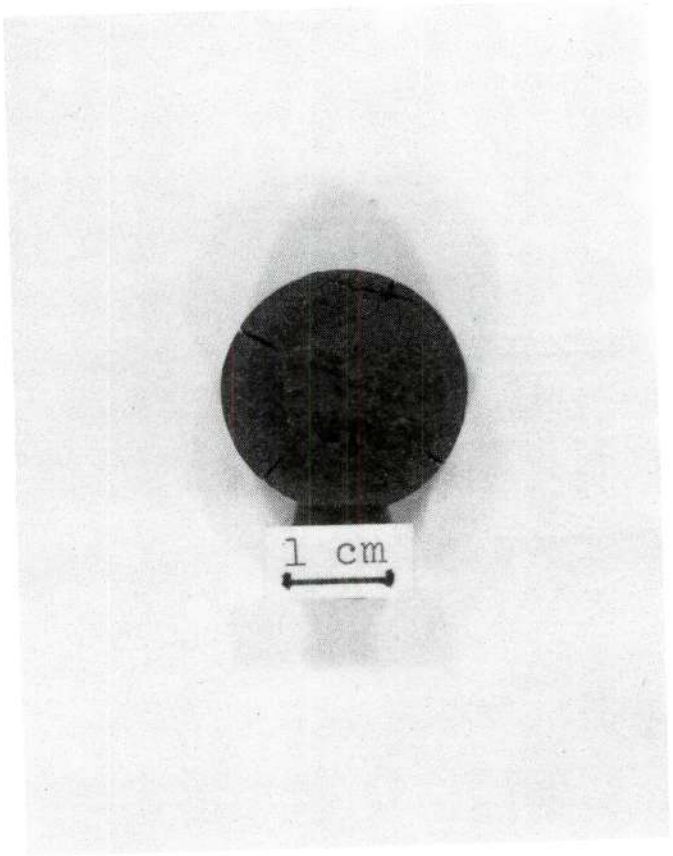


Figure 24. Transverse View of Sample LBH-6, Showing Stress-Relief Gaps and Distorted Solidified Zone

by the eight grooves, but was greatly reduced in size, indicating that the loss of heat through the grooves was substantial. Extrapolation suggests that a large number of shallow grooves may greatly improve the cracking characteristics of samples.

To evaluate a possible change in the solidification procedure designed to reduce the cracking found in most samples, two $UO_2$-W ingots were fabricated with properties as nearly identical as possible. In the first experiment, designated LBH-15A, the ingot was solidified in the usual fashion; the pellet was lowered into a stationary molybdenum postheater after the establishment of a stable molten zone. In the other ingot, LBH-15B, a stable molten zone was similarly established, but in that experiment, the molybdenum postheater was raised around the stationary ingot. Since the susceptor increased in temperature as it was raised into the work coil around LBH-15B, it was hoped that the technique would improve the sample cracking chracteristics by decreasing the thermal gradient in the solidified zone. However, those samples did not display a substantial difference in cracking characteristics. In LBH-15B, the solidified zone had a much more uniform shape than in LBH-15A, and the fiber growth was more uniform across transverse sections of the zone.

Samples LBH-20 and -21, described in the solidification rate section of this chapter, displayed unique cracking properties: the central, solidified zone remained intact except for a few intergranular fissures. The melted zone was completely surrounded by a circumferential crack which permitted the easy removal of the unmelted "skin" material (Figure 25).

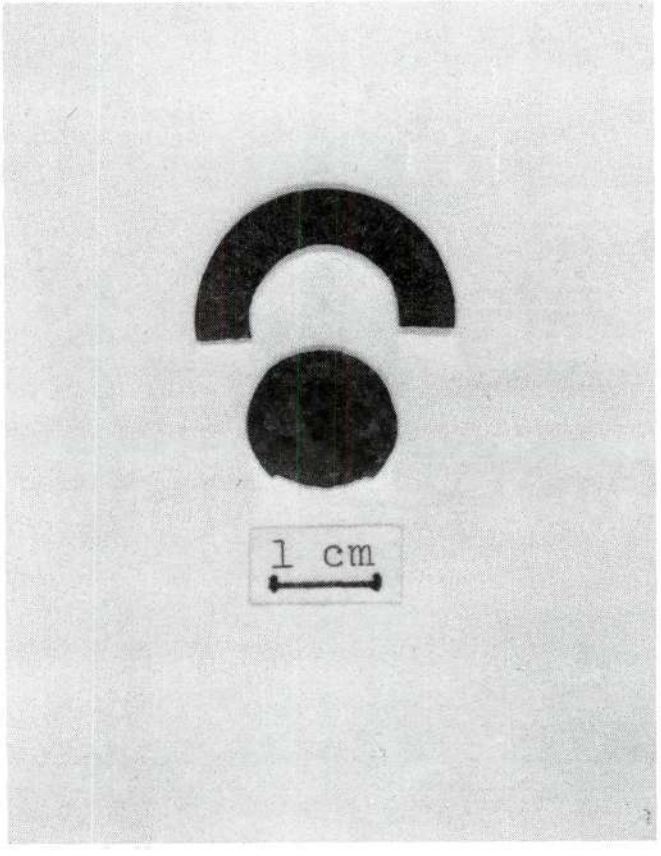


Figure 25. Photograph of Sample LBH-21 Showing Intact Central Solidified Zone and Part of the Separated "Skin" Material

Evidently, the low growth rates used in those experiments (1.5 and 0.5 cm/hr), provided a very flat solidification front, and produced a sharp interface between the central growth zone, and the surrounding skin material. In past experiments, the size of the solidified cells decreased more or less uniformly from the center to the perimeter of the samples, but in LBH-20 and LBH-21 (Figure 25), large cells were seen throughout the central core (growth region) of the sample, suggesting that decreasing the solidification rate helps alleviate cracking problems.

# CHAPTER VI

# CONCLUSIONS AND RECOMMENDATIONS

## Conclusions

1. Urania-tungsten composites can be internal-zone melted by direct induction heating using pellet diameters of 25 and 32 mm and a composition of $UO_{2.06}$-6 w/o W, after being preheated to about 1600°C, using frequencies of 3.4 and 3.1 MHz, respectively.
2. Increasing the power input to $UO_2$-W composites during unidirectional solidification tended to improve the uniformity of fiber arrays produced.
3. For unidirectional solidification of 25 mm diameter pellets, increasing the height of the 6.67 cm i.d., work coil from 7.0 to 8.25 cm, by the addition of one turn, caused larger, more stable molten zones, which led to more uniform fiber geometries.
4. Sintering $UO_{2.07}$-6 w/o W pellets in nitrogen at 1400°C for 4 hours decreased the O/U ratio to about 2.01, and yielded uniform fiber geometries when melted and unidirectionally solidified in a dynamic atmosphere of CO-1 v/o $CO_2$.
5. For 25 mm diameter sintered samples of $UO_{2.07}$-6 w/o W, the minimum density necessary for uniform fiber growth appears to be near 8.5 g/cc, or about 75% of theoretical density.
6. Perpendicular to the growth direction of unidirectionally-solidified urania-tungsten composites, fiber density variations generally decreased as the diameter of the sintered sample ingots was

increased from 16 to 25 to 32 mm.

7. As the solidification (growth) rate was decreased from 3.0 to 0.5 cm/hr, the average fiber density decreased from ∿10 million to ∿1.6 million fibers/$cm^2$ in 25 mm diameter pellets of $UO_{2.07}$-6 w/o W grown in a CO-1.0 v/o $CO_2$ atmosphere.

8. Internal cracking of unidirectionally-solidified $UO_2$-W composites can be reduced by cutting expansion grooves in the surface of the pellets. A large number of narrow grooves appears to affect the molten zone shape and size less than a few wide grooves.

9. After reduction in hydrogen, and quenching in dry ice, urania will oxidize at room temperature, in air, to an O/U ratio of ∿2.04-2.07, and can be stored in dry conditions for up to 1000 hours without undergoing substantial stoichiometry changes.

## Recommendations

Of all the parameters considered in this study, the most critical to urania-tungsten composite growth was control of the oxide stoichiometry by atmosphere manipulation. Throughout the experimental procedure, from the reduction of the as-received powder, through the sintering of the pellet, and then during the solidification process itself, the $UO_2$ undergoes more or less continual variation of its O/U ratio. That problem was augmented by the association/dissociation reactions taking place in the CO/$CO_2$ atmospheres used.

It would be preferable to utilize a non-reactive gas mixture, for stoichiometry control. All sintering and growth atmospheres must be manupulated so that that O/U ratio of the sample remains in a nearly

equilibrium condition throughout its processing. Computer control of atmosphere sampling and adjustment is advisable due to the frequency and sensitivity necessary. More powerful inductive heating units would allow the melting of larger samples, which would help dampen the effects of minor variations in atmospheric oxygen potential by providing greater masses of molten material.

Once atmospheric, and hence, stoichiometric stability, is reached, the roles of the more readily varied parameters, such as metal content and growth rate, can be better understood and controlled to produce extensive arrays of uniform fiber geometries.

# APPENDIX A

## Raw Material Characterization and Properties

The tungsten powder used in the preparation of $UO_2$-W samples was a 99.9% pure batch obtained from Teledyne Wah Chang. Since it was used consistently in all experiments, the possibility of any variation in metal powder characteristics was eliminated.

The influence of oxide powder properties on $UO_2$-W eutectic structures is critical. For that reason, a series of experiments were run on four different batches of $UO_2$ to assess their properties. Table 7 shows the supplier and assay date for the different powders. The sample designation A through D will be referred to in subsequent tests. The assay date is the date on which the radioactivity of the powder was last determined by the supplier. Sample A was from the $UO_2$ supply that has been at Georgia Tech for several years.

Table 7. Uranium Dioxide Powders Used in Characterization Testing

| Sample | Supplier | Assay Date |
|---|---|---|
| A | Numec | 8/23/73 |
| B | Exxon Nuclear | 10/2/75 |
| C | B & W (Numec) | 8/21/75 |
| D | Nuclear Fuel Services | 10/29/75 |

The following section initially discusses the errors associated with determining the oxygen-to-uranium (O/U) ratios of these powders. Next, a description of the room temperature oxidation characteristics, typical of storage conditions, is considered. The moisture content of the various powders and the oxidation behavior of the material at 80°C were determined. The sintering behaviors of the different powders were evaluated, and a cursory comparison of particle sizes and shapes was accomplished in the scanning electron microscope.

## Determination of the Oxygen-To-Uranium (O/U) Ratio

Uranium dioxide is a nonstoichiometric solid solution which will slowly oxidize in air. The determination of the O/U ratio is done by a standard gravimetric method. The $UO_{2\pm x}$ is weighed in a platinum crucible, oxidized to $U_3O_8$ in air at 800°C, and reweighed. The weight gain is assumed to be entirely from oxidation so the O/U ratio can be calculated using the atomic weights. There are two main sources of error in this measurement: 1) weighing errors, and 2) moisture on the powder.

Weighing errors, zero drift in the balance, etc., can be assumed to be $\pm$0.0004 grams. A typical error analysis calculation gives an O/U ratio accuracy of $\pm$0.002 for a powder with an O/U ratio of 2.050. This error is much less than that caused by absorbed moisture on the powder.

Calculation of the error due to moisture on the $UO_2$ is much more complicated due to the inability to determine the exact amount of water on the powder. Standard drying methods involving heating cause a change in the O/U ratio so any weight change cannot be attributed solely to the water. Drying methods at room temperature remove most of the water,

but leave a slight amount of absorbed water on the surface. Since the water content of some of the as-received powder was believed to be at least 0.1%, that parameter may have significant effect on the O/U ratio determination. Any moisture would increase the calculated O/U ratio when the weight gain was assumed to be solely caused by oxidation. Table 8 shows the effect of various moisture amounts on the apparent O/U ratio for five different starting values. The moisture content is expressed as percent (on a dry basis).

$$\frac{\text{Weight } H_2O}{\text{Weight Dry } UO_{2\pm x}} \times 100\% \qquad \text{(Eq.2)}$$

The table shows, for example, that a powder containing 0.2% moisture with a true O/U value of 2.0508 will yield an apparent O/U value of 2.0685. That error in O/U ratio is expected to be about $\pm 0.01$ to $\pm 0.03$ for most "moist" $UO_2$ powders.

The O/U ratios given in this report were calculated without any attempt to correct for the expected increase due to moisture. When interpreting the data, one is advised to consider this effect, especially for the "as-received" and "$H_2$-reduced" powders. The sintered bulk $UO_2$ pellets were essentially dry and not subject to this error.

## Storage of "As-Received" Powders

Three hundred-gram batches of the four "as-received" $UO_2$ powders were stored in glass jars in order to establish a uniform treatment procedure. One- to two-gram samples were taken from each jar for O/U ratio determinations. Three weeks and eight months later, similar groups of samples were tested in order to detect any change in stoichiometry during

Table 8. Effect of Moisture on the Calculation of the Oxygen-to-Uranium Ratio

| | O/U Ratios | | | | | | | | |
|---|---|---|---|---|---|---|---|---|---|
| | TRUE (dry) | APPARENT VALUES BECAUSE OF MOISTURE CONTENT | | | | | | | |
| Moisture Content | 0.00% | 0.1% | 0.2% | 0.3% | 0.4% | 0.5% | 1.0% | 1.5% | 2.0% |
| | 1.9998 | 2.0174 | 2.0333 | 2.0509 | 2.0668 | 2.0845 | 2.1691 | 2.2520 | 2.3368 |
| | 2.0508 | 2.0685 | 2.0845 | 2.1022 | 2.1181 | 2.1358 | 2.2207 | 2.3039 | 2.3889 |
| | 2.1005 | 2.1182 | 2.1342 | 2.1520 | 2.1679 | 2.1857 | 2.2709 | 2.3543 | 2.4395 |
| | 2.1504 | 2.1682 | 2.1843 | 2.2021 | 2.2181 | 2.2359 | 2.3213 | 2.4050 | 2.4904 |
| | 2.1990 | 2.2168 | 2.2329 | 2.2508 | 2.6680 | 2.2847 | 2.3704 | 2.4542 | 2.5400 |

storage. Table 9 gives these results.

Table 9. Room Temperature Oxidation Characteristics of Urania Powders

| Power Supplier | O/U Ratio 11/14/75 | 12/6/75 | 7/12/76 | % Increase for 8 mos. |
|---|---|---|---|---|
| A-Numec | 2.270 | 2.283 | 2.289 | 0.837 |
| B-Exxon Nuclear | 2.111 | 2.122 | 2.128 | 0.805 |
| C-B&W (Numec) | 2.104 | 2.111 | 2.135 | 1.473 |
| D-Nuclear Fuel Services | 2.160 | 2.156 | 2.165 | 0.231 |

Samples A, B, and C showed a slight increase in O/U ratio as expected due to the slow, natural oxidation processes occurring at room temperature. Sample D displayed an unexplained small decrease in O/U ratio.

## Moisture Content Determination

In order to determine the moisture content of the as-received $UO_{2+x}$ powders, a two-gram sample of each was placed in a porcelain ignition crucible and stored in a desiccator with Drierite desiccant. An empty crucible was used as a control. Sample A showed a weight loss of 0.16% which can be attributed to the drying of the powder. All of the other samples showed only very small weight changes which were within the weighing error. Those samples (B,C, and D) were assumed to be essentially dry.

## Determination of Oxidation Properties

Oxidation characteristics of the "as-received" powders (with

different starting O/U ratios) were studied by placing the powders in a drier held at 80°C and the O/U ratio measured at intervals. Figure 26 shows the oxidation curves for the different powders. Samples A showed a decrease in the apparent O/U ratio during the first 24 hours due to the drying of the powder. Samples B, C, and D showed only the slow rise in O/U ratio due to oxidation and no weight decrease because they were essentially dry at the beginning of the experiment. The comparison of powder oxidation behaviors agreed with the moisture content evaluation reported in the previous section.

Although that information was useful, for most $UO_2$-W composite growth experiments, it was necessary to have urania with an intermediate O/U ratio, such as 2.04 or 2.07. Accordingly, a sample of the Exxon powder was reduced in $H_2$ at 600°C to an O/U ratio of 2.00. It was then quenched in dry ice and allowed to oxidize until all of the dry ice had sublimed. The powder was then stored in a desiccator to limit moisture absorption. The O/U ratio after reduction was 2.0548 and after 1003 hours of storage, the O/U ratio had increased to 2.0697. In previous composite growth studies (8,30), it was found that urania powders with starting O/U ratios between 2.04 and 2.07 generally yield "good" eutectic structures, and hence storage under these conditions appears satisfactory.

## Sintering Properties

Pellets of each "as-received" powder, weighting 50 grams, were pressed in a 3/4 inch die under a 2000 lb. load. After pressing, the pellets were sintered in $N_2$ inside a Mo preheater using the Lepel rf generator under conditions identical to the preheat period used in small-

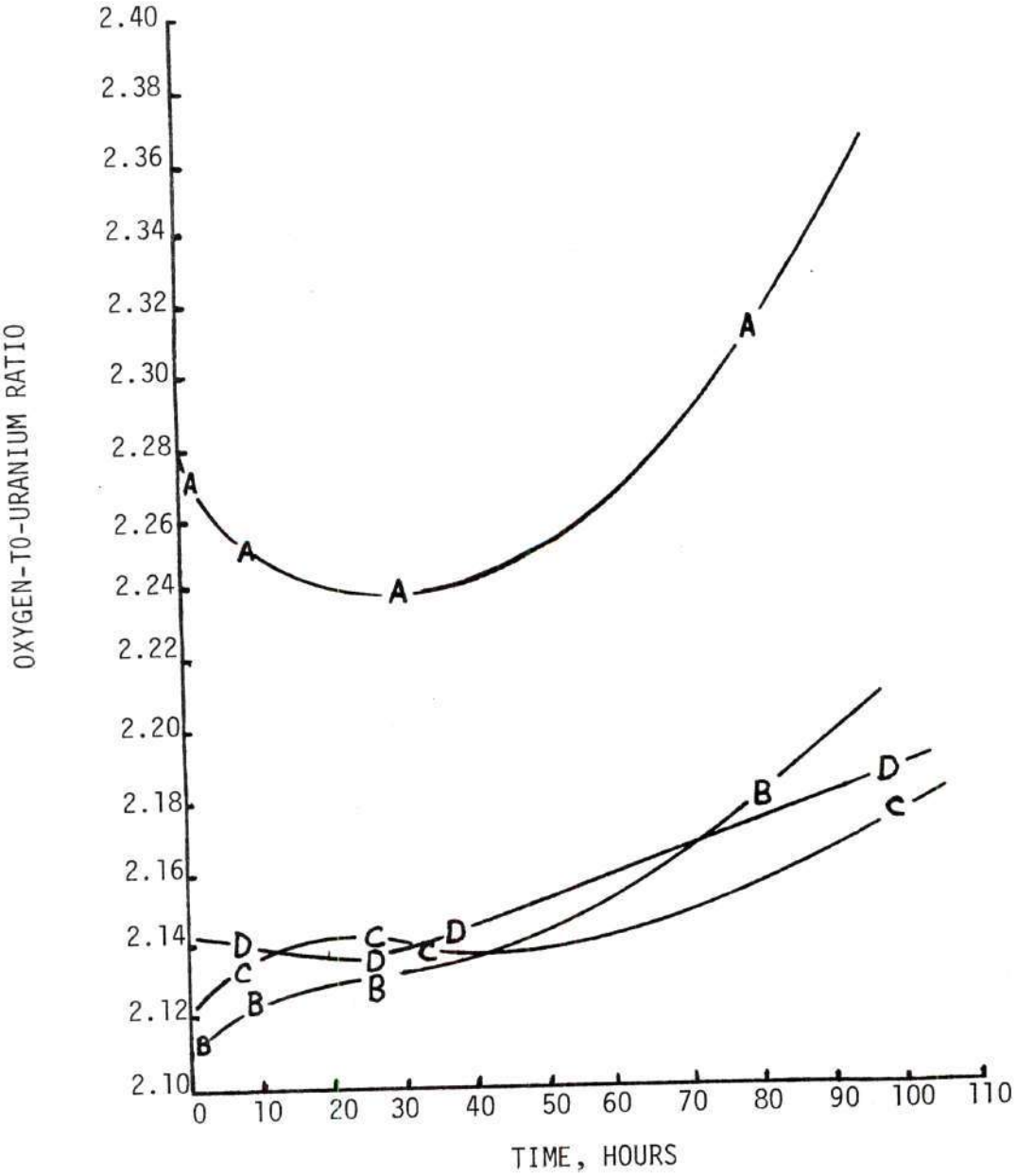


Figure 26. Oxidation of $UO_{2+x}$ Samples In Drier at 80°C

diameter $UO_2$-W composite growth experiments. The results are tabulated in Table 10.

## Particle Size Measurement

In order to get an initial estimate of the particle size and shapes of the different $UO_2$ powders, samples were mounted for scanning electron microscopic examination by placing a drop of $UO_2$-water suspension on an SEM stub and drying. Comparative analysis of poor resolution SEM micrographs provided only very general information and indicated the average particle size of all the powders was about 0.3 μm. The particles in Sample B appeared to be much more agglomerated than those in the remaining powders.

## Impurities

Spectrographic analyses of the four urania samples were conducted at Oak Ridge National Laboratory. The results are listed in Table 11.

Since there was a lack of substantial performance difference between the urania samples, cost and availability factors revealed in the choice of the Exxon powder for the majority of experiment runs.

Table 10. Results of $UO_2$ Sintering Tests

| Sample | As-Received O/U | Fired O/U | Weight Loss on firing (%) | Longitudinal Shrinkage (%) | Diameter Shrinkage (%) | Green Density (gm/cc) | Fired Density (gm/cc) |
|---|---|---|---|---|---|---|---|
| A | 2.2699 | 2.179 | 0.77 | 26.2 | 28.0 | 3.56 | 9.23 |
| B | 2.1108 | 2.113 | 0.22 | 23.7 | 24.3 | 4.04 | 9.20 |
| C | 2.106<br>2.1043 | 2.083 | 0.27 | 24.8 | 26.5 | 3.71 | 9.12 |
| D | 2.160<br>2.1604 | 2.124 | 0.33 | 24.3 | 25.6 | 4.07 | 9.68 |

Table 11

Spectrographic Analysis of Uranium Dioxide Powders*
Used in Characterization Testing,
Microgram of Element per Gram of Uranium Metal

| | Uranium Dioxide Powders | | | | |
|---|---|---|---|---|---|
| Element** | A | B | C | D | E |
| Al | < 2 | 8 | 8 | 10 | 10 |
| B | < 0.1 | < 0.1 | < 0.1 | < 0.1 | < 0.1 |
| Ba | < 1 | < 1 | < 1 | < 1 | < 1 |
| Be | < 0.1 | < 0.1 | < 0.1 | < 0.1 | < 0.1 |
| Bi | < 1 | < 1 | < 1 | < 1 | < 1 |
| Ca | < 2 | < 2 | 5 | < 2 | 8 |
| Cd | < 0.1 | < 0.1 | < 0.1 | < 0.1 | < 0.1 |
| Co | < 1 | < 1 | < 1 | < 1 | < 1 |
| Cr | < 2 | < 2 | 10 | 5 | 10 |
| Cu | < 2 | < 2 | < 2 | < 2 | < 2 |
| Fe | 10 | < 5 | < 5 | < 5 | 30 |
| Li | < 2 | < 2 | < 2 | < 2 | < 2 |
| Mg | < 2 | < 2 | 2 | < 2 | < 2 |
| Mn | < 2 | < 2 | < 2 | < 2 | < 2 |
| Mo | < 2 | < 2 | < 2 | < 2 | < 2 |
| Na | 10 | 25 | 7 | 15 | 7 |
| Ni | < 2 | < 2 | 5 | 10 | 5 |
| P | <40 | <40 | <40 | < 40 | <40 |
| Pb | < 2 | < 2 | < 2 | < 2 | < 2 |
| Sb | < 5 | < 5 | < 5 | < 5 | < 5 |
| Si | < 2 | 15 | 50 | 60 | 60 |
| Sn | < 2 | < 2 | < 2 | < 2 | < 2 |
| Y | < 2 | < 2 | < 2 | < 2 | < 2 |
| Zn | < 20 | <20 | <20 | < 20 | <20 |

*Supplier
- A Numec
- B Exxon Nuclear
- C Babcock & Wilcox (old Numec)
- D Nuclear Fuel Services
- E Same as C for reproducibility check

** < means below detection limit

# APPENDIX B

## Parameters and Results of Growth Runs

The following is a list of comments used to briefly describe the results of the various growth runs listed in Table 12. For convenience, certain data from this section appears as smaller tables throughout the discussion of results.

### Comment Codes

1. Upper and lower susceptors used (spacing in mm)
2. Banded
3. Good growth(avg. fiber density in $10^6$ pins/$cm^2$)
4. Irregular growth(avg. fiber density of good areas in $10^6$ pins/$cm^2$)
5. No growth
6. Two molten zones established
7. No stable molten zone established
8. "Blue" phase ($U_xWO_3$) present
9. O/U high, sintered with LBH-5
10. Sintered in $H_2/N_2$ atmosphere
11. Sintered in $CO_2$ atmosphere
12. Growth atmosphere CO-0.5 v/o $CO_2$
13. 1.5 inch diameter pellets
14. Susceptor raised slowly to prevent cracking
15. Expansion gaps (size in mm) cut to lessen cracking
16. Circumferential cracking occurred

Table 12. Parameters and Results of Growth Runs

| Run LBH- | Starting O/U | Composition Wt. % W | Control O/U | Sample Density(g/cc) green | fired | Growth Rate (cm/hr) | Power kV | Settings A | Comments |
|---|---|---|---|---|---|---|---|---|---|
| 1 | 2.04 | 6 | 2.01 | 4.5 | 9.1 | 2.47 | 5.6 | 0.85 | 1(25),2 |
| 2 | 2.04 | 6 | 2.01 | 4.7 | 9.9 | 2.24 | 5.7 | 0.85 | 1(25),2 |
| 3 | 2.07 | 6 | 2.01 | 4.7 | 9.2 | 3.40 | 3.7 | 0.70 | 3(7),6 |
| 4 | 2.07 | 6 | 2.01 | 4.7 | 9.3 | 2.77 | 4.6 | 0.92 | 3(10),6 |
| 5 | 2.20 | 12 | 2.09 | 4.3 | 9.0 | 2.74 | 4.0 | 0.95 | 5,7,8 |
| 5A | 2.07 | 6 | 2.09 | 4.6 | 9.2 | 2.80 | 4.7 | 0.95 | 3(12),8,9 |
| 6 | 2.07 | 6 | 2.01 | 4.6 | 9.4 | 2.87 | 4.8 | 0.95 | 3(25),8,15(0.03x5) |
| 7 | 2.07 | 4 | 2.01 | 3.8 | 8.8 | 6.00 | 4.7 | 0.95 | 4(30) |
| 8A | 2.07 | 6 | 2.01 | 4.2 | 8.0 | 2.67 | 4.6 | 0.95 | 5,7 |
| 8B | 2.07 | 6 | 2.01 | 4.4 | 8.3 | 2.67 | 4.8 | 0.95 | 4(Not Determined)7 |
| 8C | 2.07 | 6 | 2.01 | 4.6 | 8.6 | 3.20 | 4.5 | 0.95 | 3(3),6 |
| 9 | 2.07 | 6 | 2.01 | 4.6 | 8.5 | 2.95 | 5.1 | 1.00 | 3(10),8,15(1x3) |
| 10A | 2.07 | 6 | 2.01 | 4.7 | 8.5 | 2.67 | 5.2 | 1.00 | 4(30),8 |
| 10B | 2.07 | 4 | 2.01 | 4.6 | 8.4 | 2.74 | 5.1 | 1.00 | 4(6) |
| 11 | 2.07 | 6 | 2.01 | 4.6 | 10.1 | 3.18 | 5.5 | 1.05 | 3(Not Determined)13 |
| 12 | 2.07 | 6 | 2.01 | 4.6 | 10.1 | 3.33 | 5.8 | 1.10 | 3(Not Determined)13 |

Table 12 (continued)

| Run LBH- | Starting O/U | Composition Wt. % W | Control O/U | Sample Density(g/cc) green | fired | Growth Rate (cm/hr) | Power kV | Settings A | Comments |
|---|---|---|---|---|---|---|---|---|---|
| 13 | 2.07 | 6 | 2.01 | 4.5 | 9.4 | 3.50 | 5.0 | 1.00 | 3(8) |
| 14 | 2.07 | 6 | 2.01 | 4.7 | 9.6 | 2.00 | 6.0 | 0.90 | 1(25),2 |
| 15A | 2.07 | 6 | 2.01 | 4.7 | 9.6 | 3.00 | 5.0 | 1.00 | 3(12) |
| 15B | 2.07 | 6 | 2.01 | 4.7 | 9.5 | 3.00 | 4.7 | 1.00 | 3(10),14 |
| 16 | 2.07 | 6 | 2.00 | 4.7 | 8.7 | 2.31 | 5.0 | 1.00 | 5,10 |
| 17 | 2.07 | 6 | 2.01 | 4.6 | 9.9 | 3.14 | 5.3 | 0.59 | 1(36),2 |
| 18 | 2.07 | 6 | 2.01 | 4.7 | 9.8 | 2.22 | 4.8 | 1.00 | 3(Not Determined) |
| 19 | 2.07 | 6 | 2.10 | 4.7 | 9.2 | 2.00 | 4.6 | 1.00 | 3(Not Determined)11 |
| 20 | 2.07 | 6 | 2.01 | 4.8 | 10.3 | 1.50 | 5.2 | 1.00 | 3(5),12,16 |
| 21 | 2.07 | 6 | 2.01 | 4.7 | 9.8 | 0.50 | 5.0 | 1.00 | 3(1,6),16 |

# BIBLIOGRAPHY


1. C. A. Tudbury, Basics of Induction Heating, Vol. I, J. F. Ryder, Inc., 1960

2. D. Venable and T. P. Kinn, "Radio Frequency Heating," in Industrial Electronics Reference Book, Edited by Electronics Engineers of Westinghouse Electronic Corporation, John Wiley and Sons, Inc., p. 348, 1948.

3. M. D. Pao, "Unidirectional Solidification of $UO_2$-RO Type Refractory Oxides with Emphasis in the System $UO_2$-MgO," Masters Thesis, School of Ceramic Engineering, Georgia Institute of Technology, May 1973.

4. M. W. Watson,"Stabilized $ZrO_2$-W Composites Produced by Unidirectional Solidification," Masters Thesis, School of Metallurgy, Georgia Institute of Technology, December 1973.

5. J. W. Stendera, "Unidirectional Solidification of Rare-Earth Oxide-Metal Composites," Masters Thesis, School of Ceramic Engineering, Georgia Institute of Technology, September 1974.

6. B. Gayet, J. Holder, and G. Kurka, "Melting $UO_2$ By Direct High Frequency Induction," C.E.A., Direction des Materiaux et Combustibles Nucleaires.

7. D. N. Hill,"Internal Zone Melting of Refractory Oxides Using Induced Eddy-Current Heating," Masters Thesis, School of Ceramic Engineering, Georgia Institute of Technology, September 1969.

8. A. T. Chapman et al., "Melt-Grown Oxide-Metal Composites,"Technical Reports 1-6, sponsored by ARPA, Contract Numbers DAAH01-70-C-1157 and DAAH01-71-C-1046, ARPA Order Number 1637, 1971-1973.

9. A. T. Chapman and G. W. Clark, "Growth of $UO_2$ Single Crystals Using the Floating Zone Technique," J. Amer. Ceramic Soc.(JACS), 48(9), 492-95.

10. R. W. Barkalow,"Unidirectional Solidification of $Y_2O_3$-stabilized $ZrO_2$," Senior Research Project, School of Ceramic Engineering, Georgia Institute of Technology, June 1975.

11. J. F. Benzel, A. T. Chapman, and J. K. Cochran, "Investigation of the Growth of Directionally Solidified Eutectics with Potential as Electron Emitters," Final Technical Report, JPL Contract Number 954193, October 1976.

BIBLIOGRAPHY (continued)

12. M. C. Pao, M. W. Watson, and A. T. Chapman, "The Unidirectional Solidification Behavior of the Binary Alkaline Earth-$UO_2$ Systems," Fourth Intl. Conf. on Crystal Growth, Collected Abstracts, 478-479 (March 1974).

13. C. Jen, "Factors Determining the Unidirectional Solidification Behavior of the Systems $UO_2$-Ta, $UO_2$-Nb, and $UO_2$-Mo," Masters Thesis, School of Ceramic Engineering, Georgia Institute of Technology, 1972.

14. M. D. Watson, D. N. Hill and A. T. Chapman, "Solidification Behavior of Stabilized $ZrO_2$-W," JACS, (53) 112-13 (1970).

15. J. Briggs and P. E. Hart, "Refractory Oxide-Metal Eutectics," JACS, (59) 530-1 (1976).

16. E. Scheil, "Uber die eutektische Kristallisation," Zeitschrift Metallkde, (45) 298 (1954).

17. W. A. Tiller, "Polyphase Solidification," Am.Soc.Mets.Symp., Liquid Metals and Solidification, A.S.M., Cleveland, Ohio, 276-318 (1958).

18. L. M. Hogan, "The solidification of Binary Eutectic Alloys," Journal of the Australian Institute of Metals, 6 (4), 279 (1961).

19. F. L. Brady, "The Structure of Eutectics," Journal of the Institute of Metals, (28) 369 (1922).

20. A. Kofler, "Uber die Ausscheidungsanomalien in unterkuhlten binaren Schmelzen, insbesondere uber die sogenannte Hofbildung," Zeitschrift Metallkde, (40) 221 (1950).

21. J. A. Graves, "Unidirectional Solidification of $Y_2O_3$ ($CeO_2$)-Mo and $Y_2O_3$ ($CeO_2$)-W Composites," Masters Thesis, Georgia Institute of Technology, 1973.

22. R. E. Latta, R. E. Fryxell, "Determination of Solidus-Liquidus Temperatures in the $UO_{2+x}$ System ($-0.50<x<0.20$)," Journal of Nuclear Materials (35) 195-210 (1970).

23. K. Hagemark, M. Broli, "Equilibrium Oxygen Pressures over the Non-stoichiometric Uranium Oxides $UO_{2+x}$ and $U_3O_{8-z}$ at Higher Temperatures," J. Inorg. Nuc. Chem. (28) 2837-2850 (1966).

24. N. A. Javed, "Thermodynamic Study of Hypostoichiometric Urania," J. Nuc. Mat. (43) 219-224 (1972)

BIBLIOGRAPHY (continued)

25. A. T. Chapman, "Phase Relations for Cubic $UO_{2+x}$ Between 1000°C and 2900°C," Paper Presented at the Amer. Cer. Soc. 29th Pacific Coast Regional Meeting, Oct., Nov., 1976.

26. C. Jen and J. F. Benzel,"Unidirectional Solidification of the $UO_2$-Mo $UO_2$-Ta Systems," JACS, (57) 232-233 (1974).

27. T. A. Johnson and J. F. Benzel, Unidirectional Solidification of Stabilized $HfO_2$-W," JACS (56) 234 (1973).

28. J. W. Stendera and J. F. Benzel, "Rare-Earth Oxide-Metal Eutectic Composites," JACS (58) 116-19 (1975).

29. M. A. Burke, "$CeO_2$-Mo Composites Produced by Unidirectional Solidification," Master Thesis, School of Ceramic Engineering, Georgia Institute of Technology, 1974.

30. A. T. Chapman, G. W. Clark, and D. E. Hendrix, "$UO_2$-W Cermets Produced by Unidirectional Solidification," JACS, (53) 60-61 (1970).

31. R. K. Feeney, W. L. Ohlinger, A. T. Chapman, J. K. Cochran, "Investigation of Field Emission Electron Guns for Gas Lasers," Final Technical Report Sponsored by U.S.Army Missile Command, Contract Number DAAH01-74-C-0229, April 1976.